Coastal Wind Profiler Technology Evaluation

An Integrated Ocean Observing System Project
Final Report – November 2007

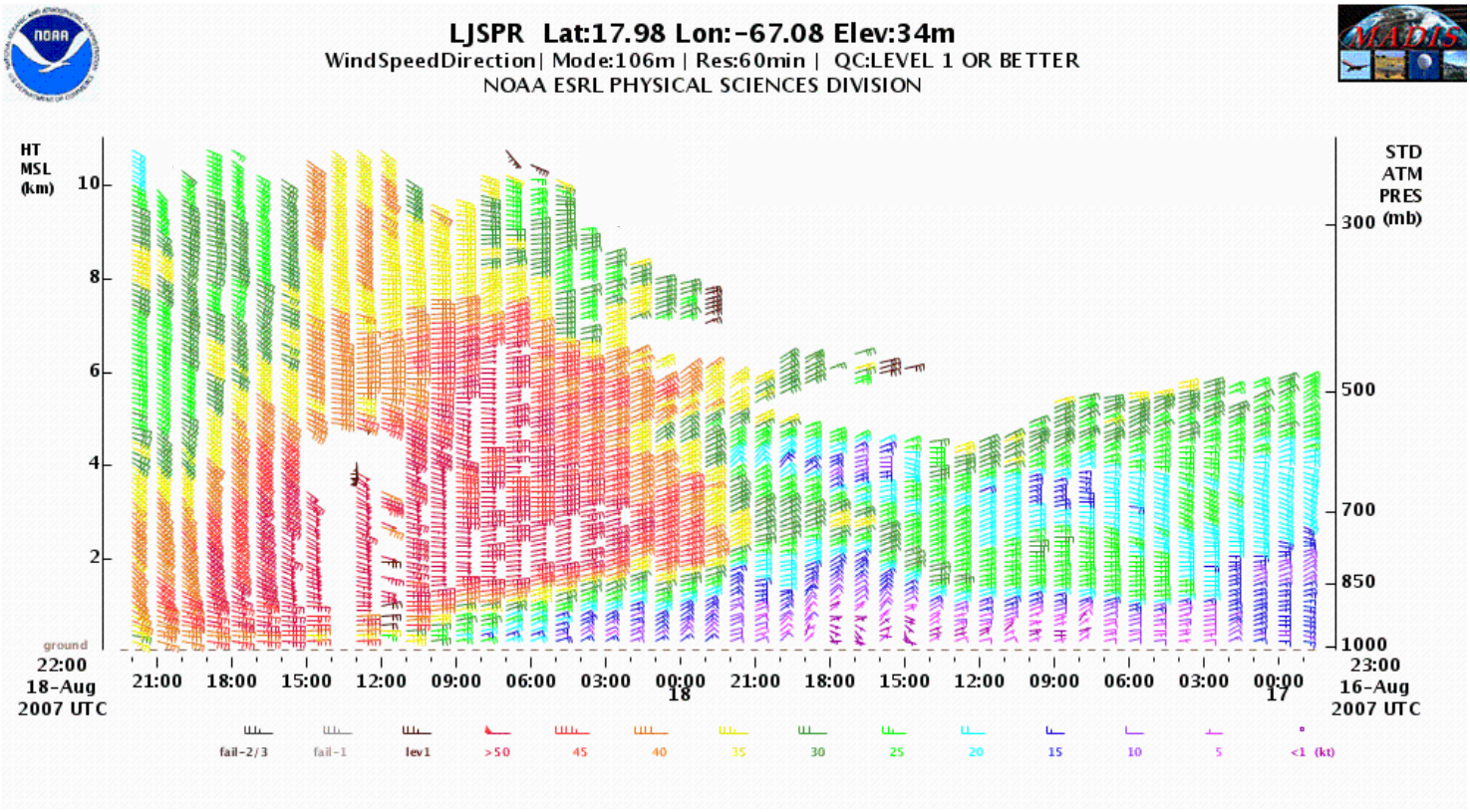

Prepared by the
NOAA Office of Oceanic and Atmospheric Research
Earth System Research Laboratory
Physical Sciences Division

Cover: Time-height cross section of winds measured by the ¼-scale 449-MHz wind profiler at La Jas, Puerto Rico, showing the high winds encountered in the outer bands of Hurricane Dean. The wind profiler was installed during July 2007 and completed a first-of-its-kind Southern U.S. wind profiler network for the U.S. Air Force's Tethered Aerostat Radar System. The image was provided by NOAA's Meteorological Assimilation and Data Ingest System (MADIS).

Time axis is from 00:00 UTC on 17 August to 22:00 UTC on August 18, 2007. Height axis is from the ground to approximately 10 km in the atmosphere. Wind speeds and directions are indicated by wind barb symbols. The wind speed is color-coded to the key along the bottom of the plot. (Courtesy of the NOAA Office of Oceanic and Atmospheric Research, Earth System Research Laboratory, Global Sciences and Physical Sciences Divisions.)

Table of Contents

List of Figures

List of Tables

1.0 Executive Summary

1.1 Overview

NOAA's coastal and marine weather prediction suffers from a lack of in situ observations. In addition many satellite algorithms fail at the coast because of the interface between the continent and the oceans. This operational gap in NOAA's observing system motivated the NOAA/OAR Earth System Research Laboratory (ESRL) to conduct an evaluation of two current, state-of-the art wind-profiler technologies to determine which technology is better suited to marine and coastal weather applications.

1.2 Methodology

The evaluation took place at the Bodega Bay Marine Laboratory north of San Francisco, California, and at the Santa Barbra Airport in Goleta, California, from September 2005 to August 2006. Two wind profilers were evaluated: the 915-MHz boundary-layer wind profiler and a ¼-scale 449-MHz wind profiler. The 915-MHz wind profiler is small, easily transportable, commercially available, and has a proven track record in coastal weather and air-quality applications. The more recently developed ¼-scale 449-MHz profiler is more expensive, commercially available, and a network of these radars recently has been installed along the Southern U.S. border and in Puerto Rico. In addition to the wind profilers, ESRL operated a radio acoustic sounding system (RASS) for temperature profiling at each of the evaluation sites. However, because simultaneous RASS measurements at the two different profiler operating frequencies could not be obtained, 915-MHz RASS data collected previously at Goleta were used to compare with 449-MHz RASS data collected during the evaluation.

Each wind profiler and RASS was evaluated based on its operating performance (e.g., minimum and maximum altitude coverage) and its ability to detect and monitor key coastal weather phenomena. Other topics that were addressed include acquisition cost, operation and maintenance issues, and frequency security.

1.3 Results

Which wind profiler and RASS provided the best maximum altitude coverage?

Using pulse coding and a 2.8 μs transmitted pulse, the Bodega Bay 449-MHz wind profiler achieved more than three times the maximum altitude coverage (6845 m vs. 2243 m above sea level)[1] of the Bodega Bay 915-MHz wind profiler using pulse coding and a 0.7 μs pulse. The 449-MHz RASS at Goleta outperformed the 915-MHz RASS at Goleta in maximum altitude coverage by nearly 700 m (1734 m vs. 1047 m above sea level).

[1] Maximum altitude coverage is defined in this report as the altitude above which valid data were retrieved less than 50% of the time.

Which wind profiler and RASS provided the best minimum altitude coverage?

For winds, the lowest range gate on the 915-MHz, 106-m operating mode was 110 m above ground. This range gate provided reliable, quality-controlled wind data 95-98% of the time. The lowest range gate on the 449-MHz, 106-m operating mode was 185 m above ground. This range gate provided reliable, quality-controlled wind data 90-95% of the time. The reduced performance of the 449-MHz wind profiler's lowest range gate is likely due to a problem with the radar's receiver described in Section 5.2 that was corrected only a few weeks into the study. The lowest range gate on the 915-MHz RASS is 135 m above ground compared to 217 m above ground for the 449-MHz RASS. For winds, the difference in minimum altitude coverage is 75 m, and for RASS, the difference is 82 m. In both cases, the 915-MHz wind profiler and 915-MHz RASS have better minimum altitude coverage.

Which wind profiler exhibited better overall time-altitude coverage for winds?

The 449-MHz wind profiler at Bodega Bay provided reliable, quality-controlled data up to 5000 m above sea level 90% of the time. The 915-MHz wind profiler at Bodega Bay provided reliable, quality-controlled data up to 1400 m above sea level 90% of the time. The ability of the 449-MHz wind profiler to obtain more reliable altitude coverage above the planetary boundary layer is due to its larger power-aperture product and longer operating wavelength, as compared to the 915-MHz wind profiler.

Which wind profiler and RASS exhibited better overall data quality?

The overwhelming impression given by the engineers and radar scientists who worked on this project is that the Doppler spectra (i.e., raw data collected by the profilers) are much cleaner for the 449-MHz wind profiler than for the 915-MHz profiler. This makes the job of signal processing much easier and should produce more robust data products. A difference in data quality was most noticeable in the observed temperature profiles from RASS, where the 449-MHz system produced much cleaner, less noisy profiles than the 915-MHz RASS.

Which wind profiler did a better job detecting gap flow conditions?

The 915-MHz wind profiler did a better job detecting the shallow gap flow phenomenon because this profiler had two range gates situated beneath the gap jet and finer vertical resolution. In contrast, the bottom gates of the 449-MHz wind profiler only were able to detect the top of the gap jet. With collocated surface wind observations, the 449-MHz profiler does an adequate job of capturing the gap flow and a much better job than the 915-MHz profiler of documenting the flow in the middle troposphere.

Which wind profiler did a better job identifying the bright band in the melting layer of precipitation?

The 915-MHz wind profiler identified 20% more bright bands than the 449-MHz wind profiler, despite the fact that the 449-MHz wind profiler ultimately was more sensitive to precipitation than the 915-MHz wind profiler. The enhanced bright-band detection capability

of the 915-MHz wind profiler resulted from two factors, namely increased vertical resolution and the absence of detectable clear-air signals during precipitation. In particular, the 63-m vertical-resolution mode of the 915-MHz wind profiler better resolved bright bands which were shallow and closer to the earth's surface. In addition, the increased sensitivity of the 449-MHz wind profiler to atmospheric turbulence often produced a second atmospheric signal peak in the Doppler spectrum that was equivalent in magnitude to the coexisting precipitation signal peak and thereby caused the spectral processing algorithm to produce, on occasion, data uncharacteristic of precipitation. While the 449-MHz wind profiler detected fewer bright bands for all precipitating conditions, it adequately detected bright bands during periods of precipitation that were deemed to be hydrometeorologically significant.

Which wind profiler did a better job measuring coastal boundary-layer depth?

Neither wind profiler technology is ideally suited to measuring the shallow marine boundary layers that often exist along the U.S. West Coast under onshore flow conditions because of insufficient vertical resolution and minimum detectable range. For deeper marine boundary layers or for boundary layers that have more of a continental influence, the 449-MHz RASS provides the most unambiguous depiction of the capping inversion defining the boundary-layer depth. Because 449-MHz RASS outperformed 915-MHz RASS in terms of altitude coverage and data quality, the 449-MHz profiler makes a slightly better, suboptimal choice for detecting and monitoring coastal boundary-layer depth. A much more suitable technology for this application is sodar, which is currently being used operationally to monitor coastal boundary-layer depth at the San Francisco Airport.

What are the relative costs to acquire, operate, and maintain each system?

The cost of buying a ¼-scale 449-MHz wind profiler with RASS (including the software required to operate the wind profiler and acquire its data) is slightly more than double the cost of buying a 915-MHz wind profiler ($620k vs. $300k; based on the commercial manufacturer's GSA price schedule). Similarly, the annual cost associated with operating and maintaining a ¼-scale 449-MHz wind profiler with RASS is slightly more than double the cost of operating and maintaining a 915-MHz wind profiler with RASS ($53k vs. $24k).

Which wind profiler operating frequency is secure for NOAA's long-term operations?

The radio spectrum in the U.S. is quite crowded and, therefore, none of the operating frequencies used for wind profiling is completely secure for long-term operations. However, the National Telecommunications and Information Administration has set aside the 448-450 MHz frequency band for wind profiling. This band is shared with amateur radio operators and the Military. If necessary, the Military can shut down other operators in this band, including NOAA profiler operators. The 915-MHz wind profilers operate in what is known as the "garbage band" (902-928 MHz). Although NTIA has granted NOAA a stage-three license for operating 915-MHz wind profilers throughout the U.S. and its possessions, the growing number of operators in this band will make it more difficult to operate 915-MHz wind profilers in the future, especially in urban areas.

2.0 Introduction

2.1 Background and Purpose of Study

This study was conducted to evaluate current, state-of-the-art wind profiler technologies for the purpose of detecting and monitoring important weather phenomena for coastal and marine weather forecast applications. Today, wind profilers are a mature technology used throughout the world (Fig. 2.1-1). NOAA Research and industry partners established a demonstration network of wind profilers in the central U.S. during the early 1990's (Fig. 2.1-2). This network is now referred to as the NOAA Profiler Network (NPN). A Cost of Operational Effectiveness Analysis (COEA) mandated by the U.S. Senate (108th Congress) was completed in 2004 to compare the "… cost to upgrade the NOAA Profiler Network (NPN) over the next decade versus the short, medium, and longterm costs of ending the NPN program." The COEA concluded that "the best combination of performance and cost is to maintain the NPN system and modify its frequency so as not to interfere with reception by SARSAT satellites of signals from Search and Rescue beacons." Furthermore, the COEA added that "while other systems have individual attributes that may exceed the capability provided by NPN, there are significant physical or cost impediments that preclude their use in lieu of NPN." Partly in response to the COEA and to other well-documented results demonstrating the impact of the NPN data on forecast improvements, NOAA operationalized the NPN in 2005.

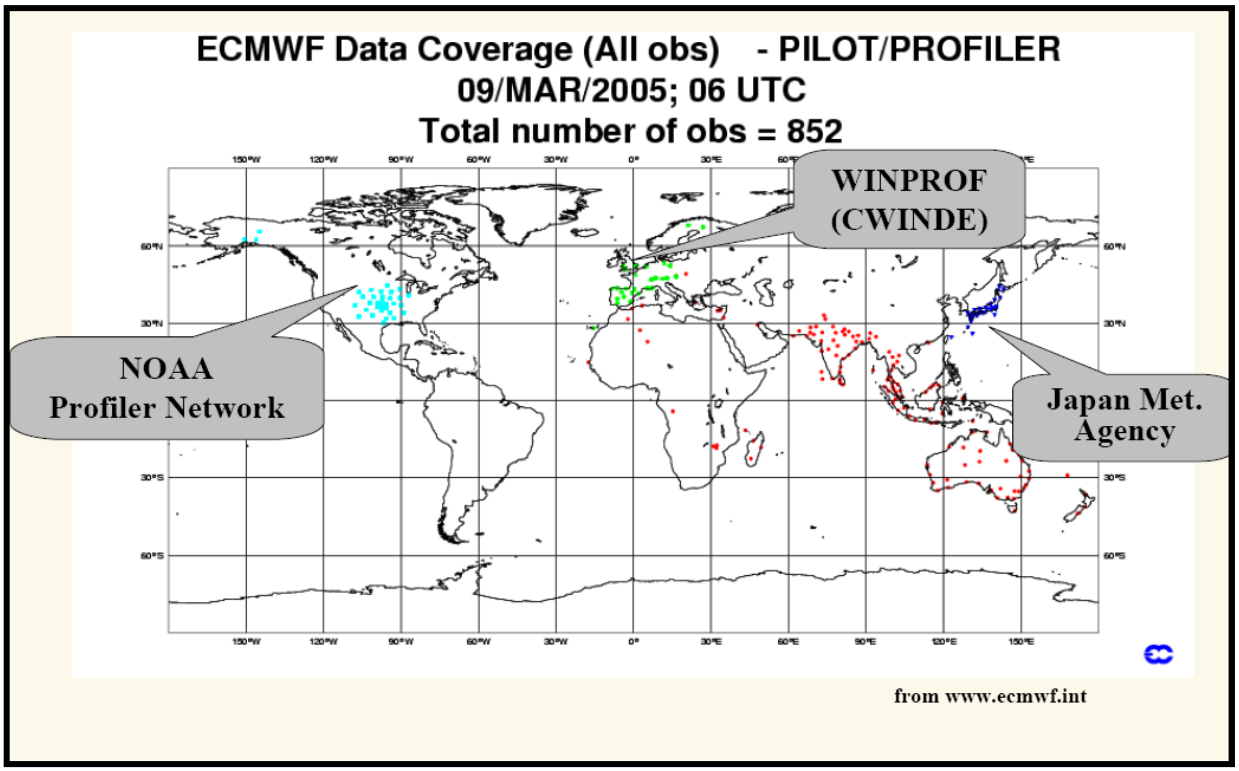

Figure 2.1-1 Worldwide wind profiler networks (colored dots) that provide data for model assimilation through the Global Telecommunication System (GTS).

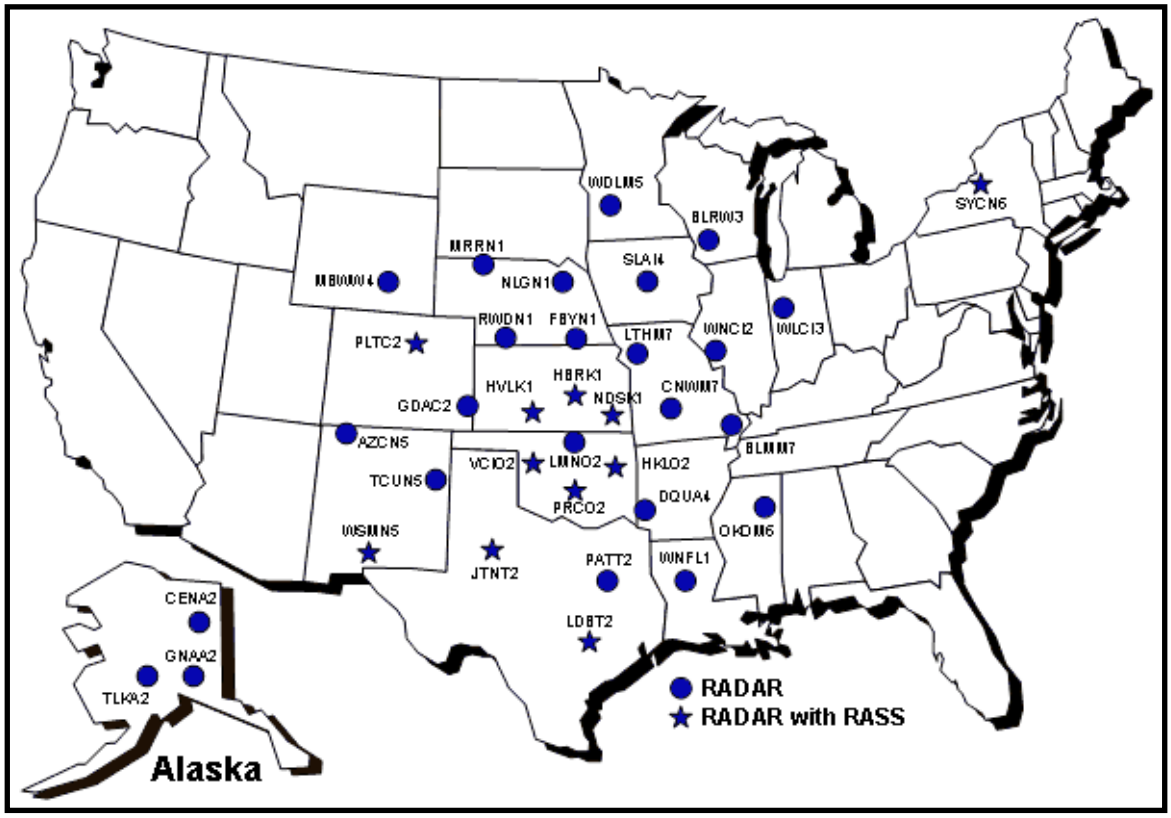

Figure 2.1-2 Map of the conterminous U.S. plus Alaska showing the locations of the NOAA Profiler Network (NPN). Sites instrumented with a wind profiler are indicated by circles. Sites instrumented with a wind profiler and a radio acoustic sound system (RASS) for temperature profiling are indicated by stars.

Figure 2.1-2 clearly indicates that none of the current NPN profilers is located in a coastal region. This is significant for the following reasons:

- Over 50% of the U.S. population lives in coastal areas that account for less than 20% of the nation's land, and coastal development still is increasing. 25% of the coast will be developed by 2025, versus 14% in 1997. As a result, more homes, businesses and lives will be vulnerable to coastal storms and more accurate forecasts will be required to reduce risks associated with hazardous weather.
- Approximately 50% of the 220 marine zones for which the NWS issues forecasts have no in-situ observations.
- Coastal storms account for 71% ($7B) of annual U.S. disaster losses. Coastal profiler networks would aid in reducing these losses by providing the NWS with the measurements necessary for improving short-term wind, precipitation, and aviation forecasts, including watches and warnings**.**

The NPN was originally designed to address forecast problems associated with convection and severe weather on the Plains. Deep vertical coverage was an important design requirement for the profiler technology used in the NPN in order to observe the deep

convection that occurs in this region. However, most atmospheric processes and the variables associated with them observed in the coastal environment are shallow in nature, e.g., marine fog, marine stratus, marine-layer depth, marine-layer advection, continental outflow through breaks in terrain, downslope winds, low-level jets, and the melting layer. To help detect and monitor these features, a wind profiler that can observe close to the ground and upward with fine vertical resolution is required. These design attributes are in conflict with the current technology used in the NPN, although at the time of this report NOAA was evaluating how to upgrade the NPN, based primarily on a mandate by the National Telecommunications and Information Administration (NTIA) to change the profiler operating frequency from 404 MHz to 449 MHz.

In FY 2005, NOAA's Integrated Ocean Observing System (IOOS) funded the NOAA/OAR Earth System Research Laboratory (ESRL), where a majority of the Nation's profiler research expertise has been assembled over the past several decades, to conduct an evaluation of current profiler technologies to determine the best match for detecting and monitoring marine and coastal weather phenomena. ESRL chose to evaluate two current wind profiler technologies at the University of California's Bodega Bay Marine Laboratory (BBY) north of San Francisco (Figs. 2.1-3). The BBY site was ideally suited for the evaluation because it experiences a wide range of weather conditions characteristic of the coastal zone, varying from shallow fog layers (Figs. 2.1-4 and 2.1-5) to intense land-falling winter storms (Fig. 2.1-6), and because a uniquely detailed understanding of the local meteorological conditions has emerged from a decade of NOAA research focused on coastal meteorology in the area (for a list of research publications resulting from this work, go to http://hmt.noaa.gov/pubs.html).

Because two radio acoustic sounding systems (RASS) could not be operated side-by-side at BBY, a second evaluation site at the Santa Barbra Airport in Goleta, California (GLA), was employed (Figs. 2.1-7 a,b). The operation of the wind profiler and RASS at GLA was cosponsored by the NOAA Coastal Storms Program (CSP), which used the profiler and RASS as part of the CSP Southern California Pilot Study. To expedite deployment of the equipment at BBY and to ensure up-to-date technology was used in the evaluation, ESRL contracted to borrow a radar antenna and transmitter from Vaisala Inc., a leading environmental measurements company that partners with ESRL on profiler technology development through a highly successful Cooperative Research and Development Agreement (CRADA).

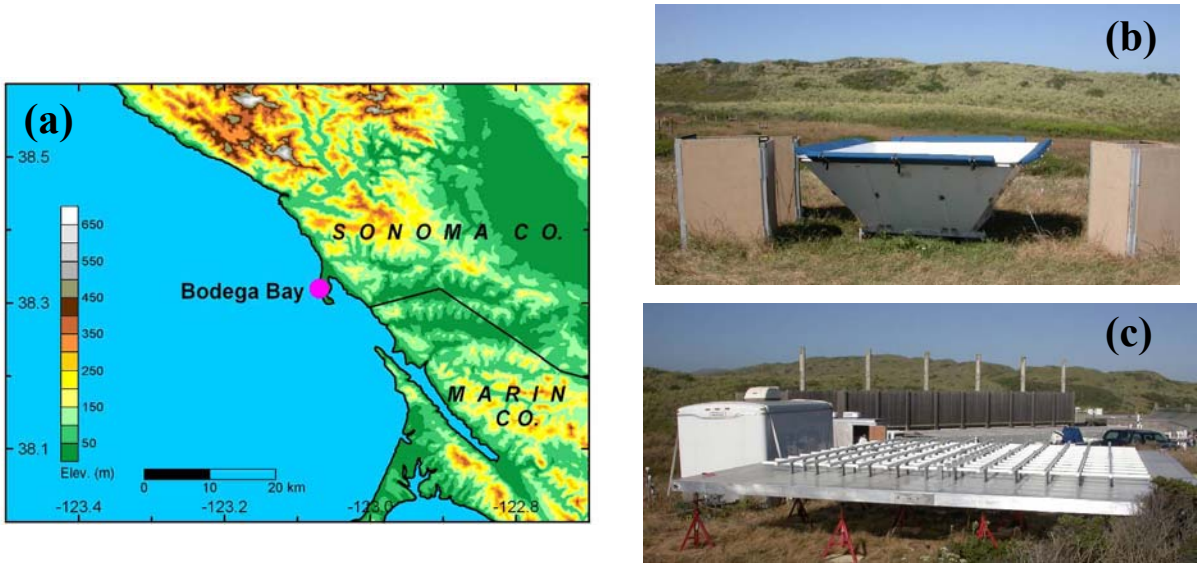

Figure 2.1-3 (a) Map showing the location of the Bodega Bay Marine Laboratory (BBY), where the primary technology evaluation took place. The (b) 915-MHz wind profiler with RASS and (c) ¼-scale 449-MHz wind profiler installed at BBY.

Figure 2.1-4 Fog conditions depicted by the web cam at BBY. The time of the image, 08:13 PDT, corresponds to 15:13 UTC.

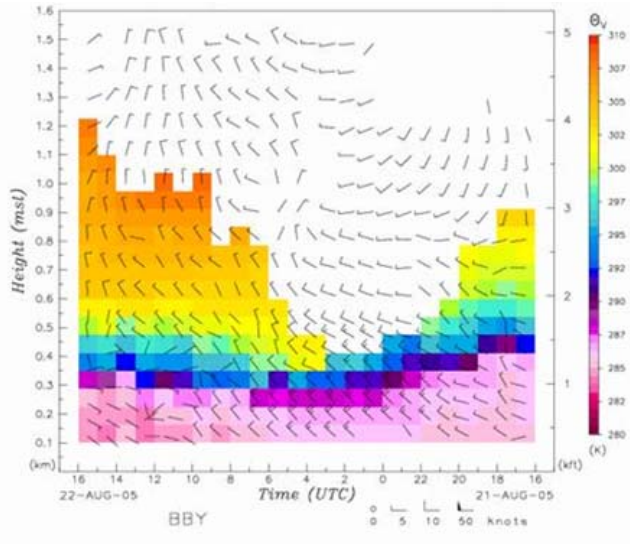

Figure 2.1-5 Time-height cross section of virtual potential temperature profiles produced by the 915-MHz RASS at BBY depicting the depth of the shallow marine layer that produced the fog show in Figure 2.1-4.

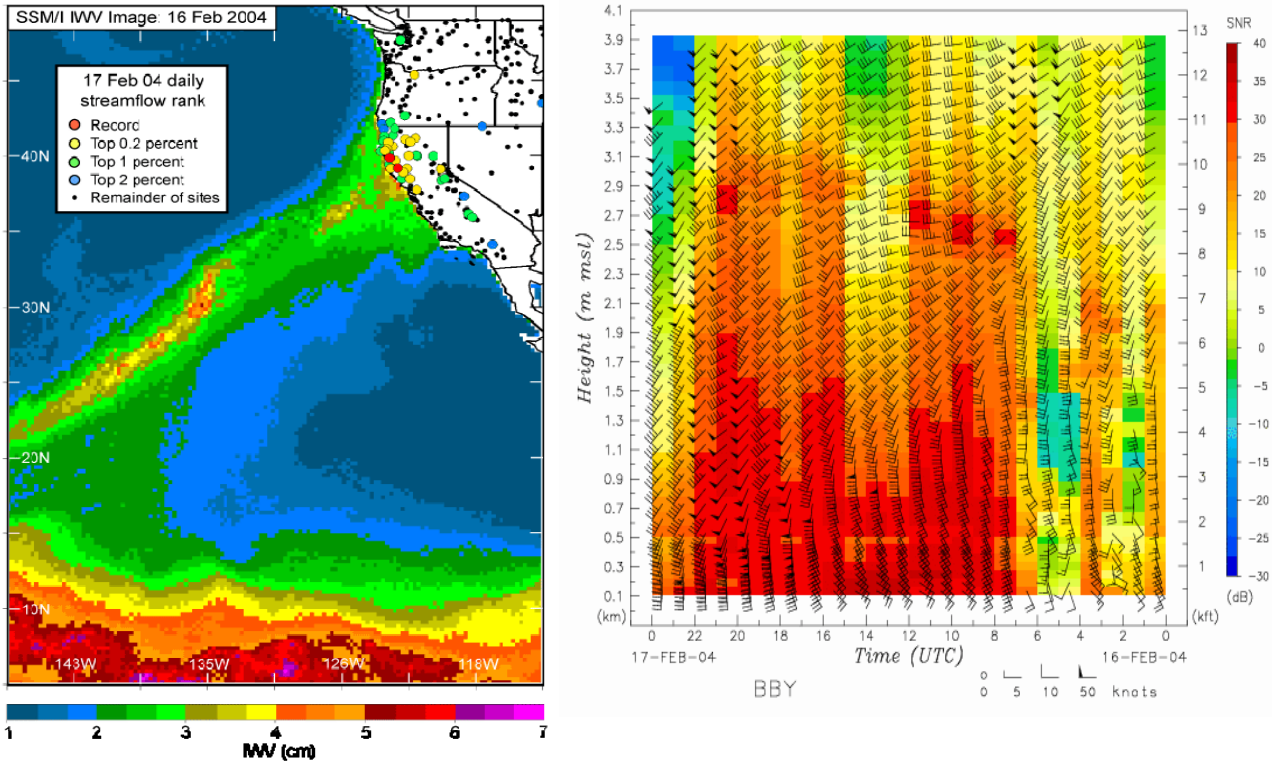

Figure 2.1-6 Composite SSM/I satellite image of integrated water vapor (IWV; left) constructed from polar-orbiting swaths on February 16, 2004. The narrow band of enhanced IWV is referred to as an "atmospheric river" and is a key feature of a powerful winter storm that struck the California coast. The accompanying flooding that occurred in the region near BBY is indicated by the stream flow ranks for rivers that had recorded > 30 years of data. Time-height cross section of wind profiles (right) measured by the 915-MHz wind profiler at BBY on February 16, 2004, before the IOOS technology evaluation started. The colored rectangles indicate the signal-to-noise ratio of the backscattered radar signals.

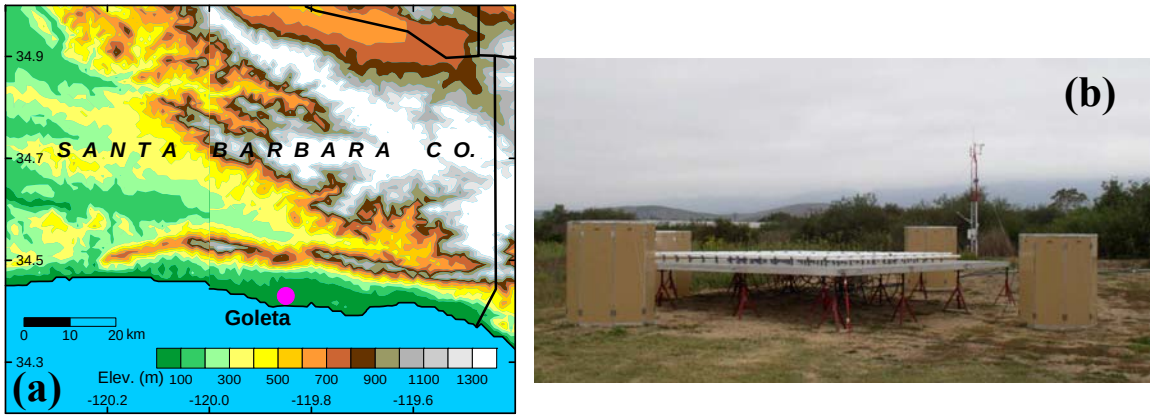

Figure 2.1-7 (a) Map showing the location of the Santa Barbra Airport in Goleta (GLA), where data from a RASS operating in conjunction with a 449-MHz profiler was collected. (b) The ¼-scale 449-MHz wind profiler with RASS installed at GLA.

2.2 Wind Profilers

Wind profilers are Doppler radars that most often operate in the VHF (30-300 MHz) or UHF (300-1000 MHz) frequency bands. There are three primary types of radar wind profilers in operation in the U.S. today. The NOAA Profiler Network (NPN) profiler operates at a frequency of 404 MHz (Table 2.2-1, Fig. 2.2-1a). The second type of profiler that is used by NOAA research and outside agencies is the 915-MHz boundary-layer profiler (Table 2.2-1, Fig. 2.2-1b). The 404-MHz profilers are more expensive to build and operate, but they provide the deepest coverage of the atmosphere. The 915-MHz profilers are smaller and cheaper to build and operate, but they lack height coverage much above the boundary layer. A third type of profiler that operates at 449 MHz (the so-called ¼-scale 449-MHz profilers) combines the best sampling attributes of the other two systems (Table 2.2-1, Fig. 2.2-1c). ESRL recently constructed and installed eight of these radars for the U.S. Air Force to assist with operation of the Tethered Aerostat Radar System used along the southern U.S. border for drug smuggling intervention (Fig. 2.2-2; for a summary of the TARS wind profiler program see http://hotitems.oar.noaa.gov/storyDetail_org.php?sid=4487. This IOOS report evaluates which of the latter two wind profiler technologies mentioned above (915 MHz and 449 MHz) is better suited to marine and coastal weather applications. The NPN 404-MHz profiler was not evaluated because, with its current design, the vertical resolution of the data and minimum detectable range are not well suited for many of the shallow phenomena that are important for coastal and marine weather.

Table 2.2-1 Physical, operating, and sampling characteristics of wind profilers.

	404-MHz (NPN)	**915-MHz (boundary layer)**	**449-MHz (quarter- scale)**
Antenna type	Coaxial-colinear phased array	Flat rectangular microstrip patch	Coaxial-colinear phased array
Antenna diameter (m)	13	2	6
Beamwidth (deg.)	4	10	10
Peak transmit power (W)	6000	500	2000
Transmit pulse width (μs)	3.3[p], 20[p]	0.417*, 0.708*,[p]	0.708*, 2.833
Height coverage (m)	500** – 16,000	120 – 4,000	180[+] – 8,000
Vertical resolution (m)	320[ᵴ], 900[ᵴ]	63, 106*	106, 212*,[ᵴ]
Temporal resolution (min)	60	60	60

* These settings reflect how the profilers were operated during the IOOS technology evaluation. Other degraded transmit and sampling resolutions are possible.

[p] Pulse-coding was used in selected operating modes to boost signal power and increase altitude coverage (for more information on pulse coding, see Ghebrebrhan, 1990).

[+] This minimum detectable range has been achieved with the ¼-scale 449-MHz profilers using a 0.7-μs pulse.

** Signal attenuators prevent accurate radar reflectivity data below 1 km.

[ᵴ] Increased vertical resolution as compared to the transmit pulse length was accomplished by oversampling.

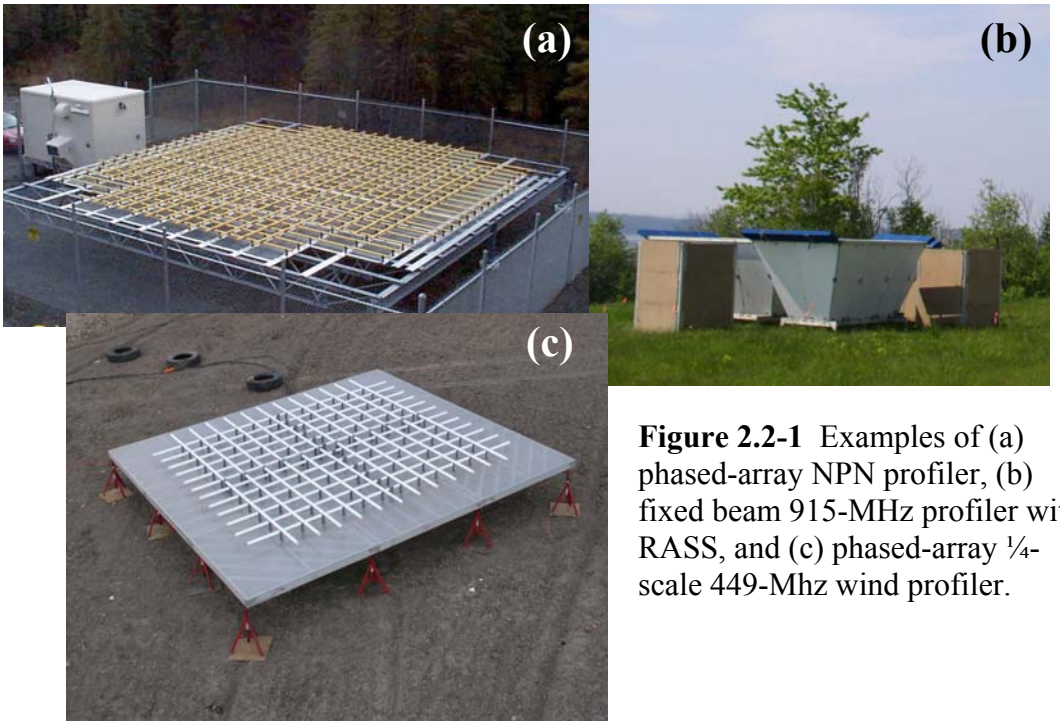

Figure 2.2-1 Examples of (a) phased-array NPN profiler, (b) fixed beam 915-MHz profiler with RASS, and (c) phased-array ¼-scale 449-Mhz wind profiler.

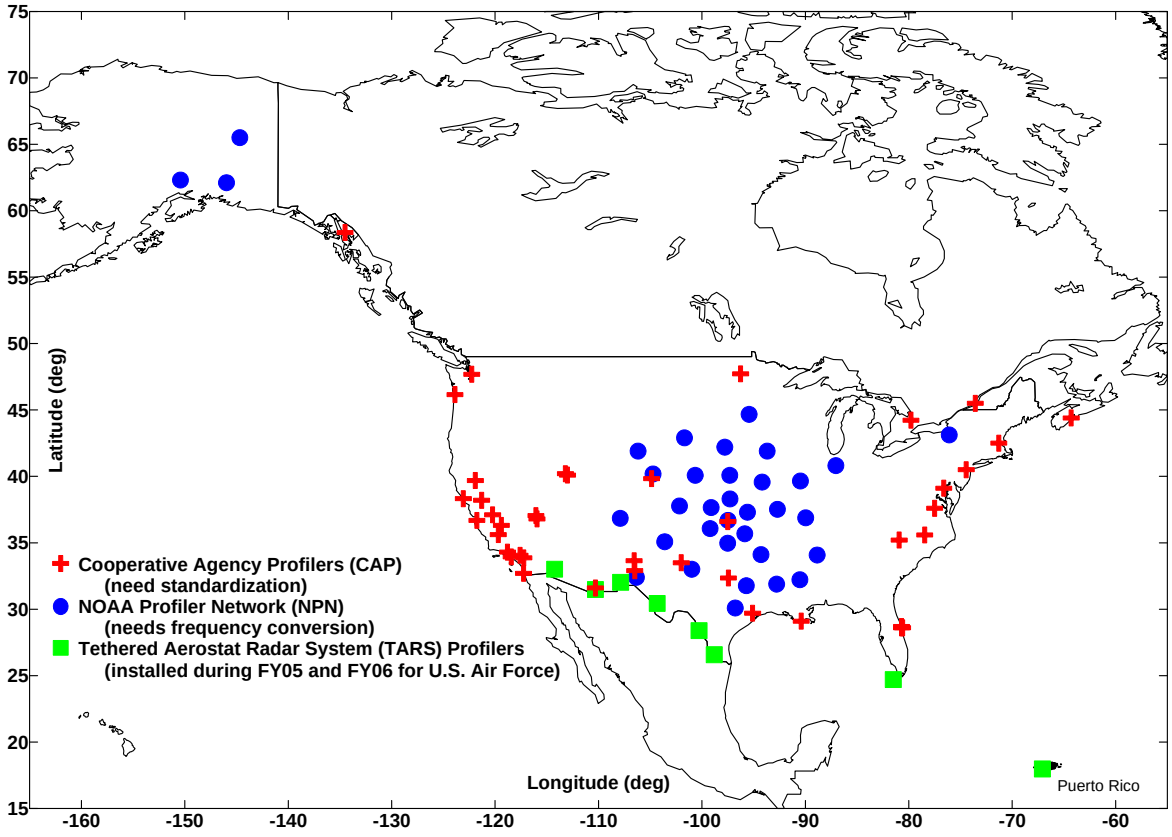

Figure 2.2-2 Map showing the locations of various U.S. and Canadian profiler networks. The locations of the recently installed TARS profilers are indicated by the green squares.

Wind profilers transmit pulses of electromagnetic radiation vertically and in at least two slightly off-vertical (~75 degree elevation) directions in order to resolve the three-dimensional vector wind. A small amount of the energy transmitted in each direction is reflected or backscattered to the radar. The backscatter returns are Doppler shifted by the motion of the scattering media. The return signals are sampled in the receiver at discrete intervals called range gates. If the sampling interval is the same as the length of the transmitted pulse, then adjacent range gates are produced. The transmit pulse is usually on the order of hundreds to thousands of nanoseconds (ns). For example, a 700 ns pulse translates into a non-oversampled range resolution of 105 m.

Profilers receive backscatter returns from atmospheric features (turbulence, clouds, precipitation) and non-atmospheric features (insects, birds, trees, airplanes, radio frequency interference). The challenge in signal processing is to avoid the returns from non-atmospheric scattering targets and focus on the atmospheric returns. To do this, profilers integrate thousands of consecutive samples to boost the signal-to-noise ratio of the atmospheric returns, a process known as coherent integration. A set of coherent integrations is processed via Fast Fourier Transform to produce a single Doppler velocity spectrum, and a set of spectra are averaged together to improve the detectability of the spectral peak. The strongest peak in the spectrum is analyzed and assumed to be the peak resulting from atmospheric backscatter. A new commercially available signal processing algorithm identifies multiple peaks and uses pattern recognition to determine which peaks are most likely to be the result of atmospheric returns.

The spectral peak is analyzed to produce a set of Doppler spectral moments, the first three of which correspond to the signal power, radial velocity, and spectral width. This is repeated for each range gate and for each of the three transmitted beam directions. A wind profile is constructed by geometrically transforming the radial velocities into the meteorological coordinate system. A single wind profile is produced over an observing period of 30 to 90 s. All of the wind profiles measured within a specified averaging period (15 min to 60 min) are averaged together using a consensus routine. The consensus routine filters outliers using threshold and acceptance windows. The consensus wind profiles are recorded on site and transmitted back to a data hub in Boulder, Colorado, via phone lines or, in remote areas, via satellite communications.

2.3 Post Data Collection Quality Control

Certain parts of the analyses presented in Section 3 used the wind profiler data collected in real time during the evaluation in order to represent the actual data that would have been available to forecasters in near-real time. Other parts of the analyses in Section 3 used wind data that were post-processed after the evaluation with the NOAA wind profiler quality control algorithms. Following is a brief description of the process used to quality control wind profiler data.

Although traditional signal-processing methods are designed to remove unwanted non-atmospheric signals from the Doppler spectrum, there are still contaminated spectral signals that produce erroneous moment-level data and, subsequently, wind profiles. Quality control algorithms are implemented to identify and remove these erroneous data that would

otherwise render inaccurate meteorological measurements and interpretation. ESRL currently uses a continuity method developed by (Weber et al., 1993) to identify and preserve only those measurements that exhibit consistency in height and time.

The continuity method is based on the fundamental assumption that some valid data are present in the comparison domain. The degree of continuity of an individual data point is established by comparing its data value with the value interpolated from neighboring data points. A data value is considered discontinuous with its neighbors if the comparison exceeds a prescribed threshold. The size of the domain used in the interpolation typically consists of two neighboring heights above and below and two neighboring times before and after. A linear least-squares interpolation is used to increase the tolerance for large slopes in the data. Therefore, meteorological features of interest, such as shears and accelerations in the wind field and temperature gradients in the vicinity of fronts, are determined to be continuous.

Because erroneous measurements can also exist in the form of continuous time-height clusters, the point-continuity test can fail to identify erroneous data values at individual data points whose comparison domains lie completely within the erroneous cluster. To combat this potential problem, the continuity algorithm uses pattern recognition to identify erroneous data clusters. Patterns in a data set are formed by identifying subsets of data that are continuously connected. Neighboring points with similar values are placed in the same branch of some pattern. Additional branches are identified when neighboring points have different values. These branches may be part of the same pattern or may belong to completely different patterns. After all of the patterns in the data set have been recognized, a series of continuity tests are performed to identify discontinuities between the different branches while attempting to preserve the largest pattern size.

These methods have produced high quality results under a variety of meteorological conditions over many months of observations. Nevertheless, certain types of contamination, such as ground and sea clutter, can persist over time with consistent Doppler shift over many heights. In these situations, the continuity method can produce undesirable results. Perhaps the combined use of the continuity method with newly developed signal-processing techniques will provide the higher levels of intelligence needed to remove even the severest types of spectral contamination.

3.0 Operating Performance

3.1 Altitude Coverage (Low and High)

The datasets used in the analysis consist of the 449-MHz wind profiler and RASS data collected at Goleta, CA (GLA), and the 915-MHz wind profiler and RASS data and the 449-MHz wind profiler data collected at Bodega Bay, CA (BBY). In addition, because two RASS systems could not be operated side-by-side at either GLA or BBY because of interference issues, we used an 11-month 915-MHz RASS dataset collected at GLA during 2001-2002 to compare against the 449-MHz RASS dataset collected during the IOOS technology evaluation. All data were processed using the NOAA wind profiler quality control algorithms (see Section 2.3). The wind datasets also were inspected visually to remove migrating bird contamination (Wilczak et al., 1995). Data passing both the quality control algorithms and the visual inspections are referred to as valid data points. The altitude coverage analyses considered the entire evaluation as well as seasonal periods for the fall (15 September through November), winter (December through February), spring (March through May), and summer (June through 15 August). Using the processed hourly-averaged wind profiler wind data and RASS virtual temperature data, ensemble-averaged datasets were created separately for the 11-month period and the four seasonal periods. Valid data points in the final datasets represent winds or temperatures where 50% or greater of the available hourly-averaged data were valid. Maximum height coverage represents the level above which less than 50% of the averaged data points were valid. Each profiler operated in two operating modes for winds and a single operating mode for RASS. For winds, the finer vertical resolution mode (63 m for the 915-MHz wind profiler and 106 m for the 449-MHz wind profiler) is referred to as the "low mode," owing to the lower maximum altitude that can be achieved using a shorter transmitted pulse, and the coarser vertical resolution mode (106 m for the 915-MHz wind profiler and 212 m for the 449-MHz wind profiler) is referred to as the "high mode." The vertical resolutions listed here and in Table 2.2-1 correspond to the vertical beam transmitted by the wind profiler. The actual vertical resolution of the wind profiles is reduced by a factor of $sin(\alpha)$, where α is the elevation angle of the off-vertical transmitted beams (66.4 degrees for the 915-MHz wind profiler and 74.7 degrees for the 449-MHz wind profilers).

BBY 449-MHz profiler winds: The results of the analysis are summarized in Table 3.1-1. The average height coverage for all data was just less than 4800 m for the low mode and just less than 6900 m for the high mode. For the high mode, the greatest height coverage occurred during the fall with the least coverage during the winter. Figure 3.1-1 shows a diurnal composite of BBY 449-MHz profiler winds for the entire evaluation. Overlaid on the time-height cross section are contours of the percentage of valid data points used to obtain the ensemble average. Notice that below 5000 m; more than 90% of the available data were valid winds. The availability of valid winds drops off linearly between 5000 and 7000 m. Westerly flow dominates at all levels and gradually decreases in speed approaching the surface. Wind barbs show no diurnal variation in height coverage. Figure 3.1-2 shows diurnal composites of BBY 449-MHz profiler winds for the winter and summer seasons. The winter season shows the dominance of westerly flow at all levels while the summer season shows the influence of the subtropical high on winds in the lowest 2000 m with prevailing southwesterlies aloft. The summer season also shows some evidence of a diurnal height

coverage variation with greater height coverage during the nighttime and early morning hours (0600-1400 UTC). Overall height coverage for the winter and summer seasons was comparable.

Table 3.1-1 BBY 449-MHz wind profiler maximum height coverage statistics.

	Fall	*Winter*	*Spring*	*Summer*	*All data*
Low mode					
Mean height (m)	5007	4696	4828	4726	4794
Standard deviation	199	186	133	126	83
High mode					
Mean height (m)	7111	6734	6760	6922	6845
Standard deviation	181	194	153	341	142

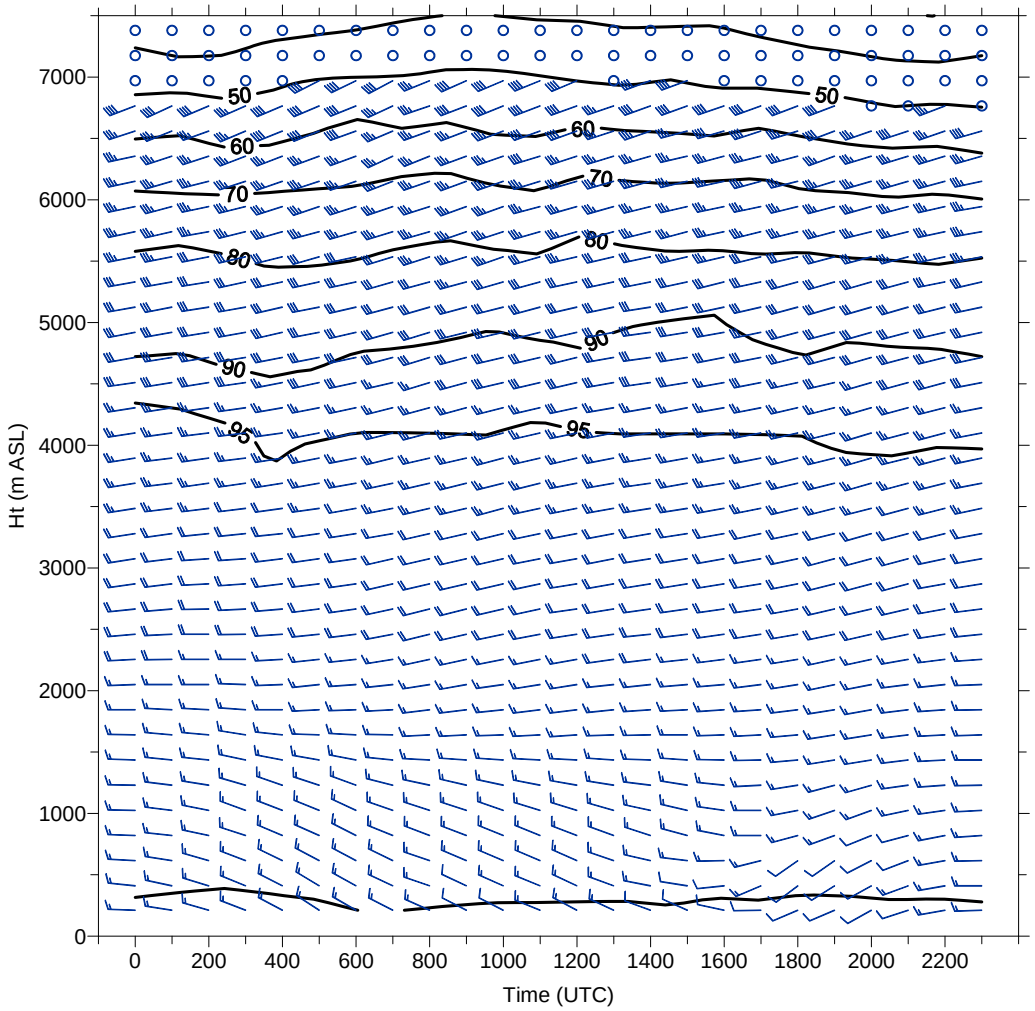

Figure 3.1-1 Diurnal composite of BBY 449-MHz wind profiles from the high mode for the entire evaluation. Contours indicate the percentage of valid data points used to obtain the composite. Wind barbs: a full barb is 5.0 m s^{-1} and a half barb is 2.5 m s^{-1}.

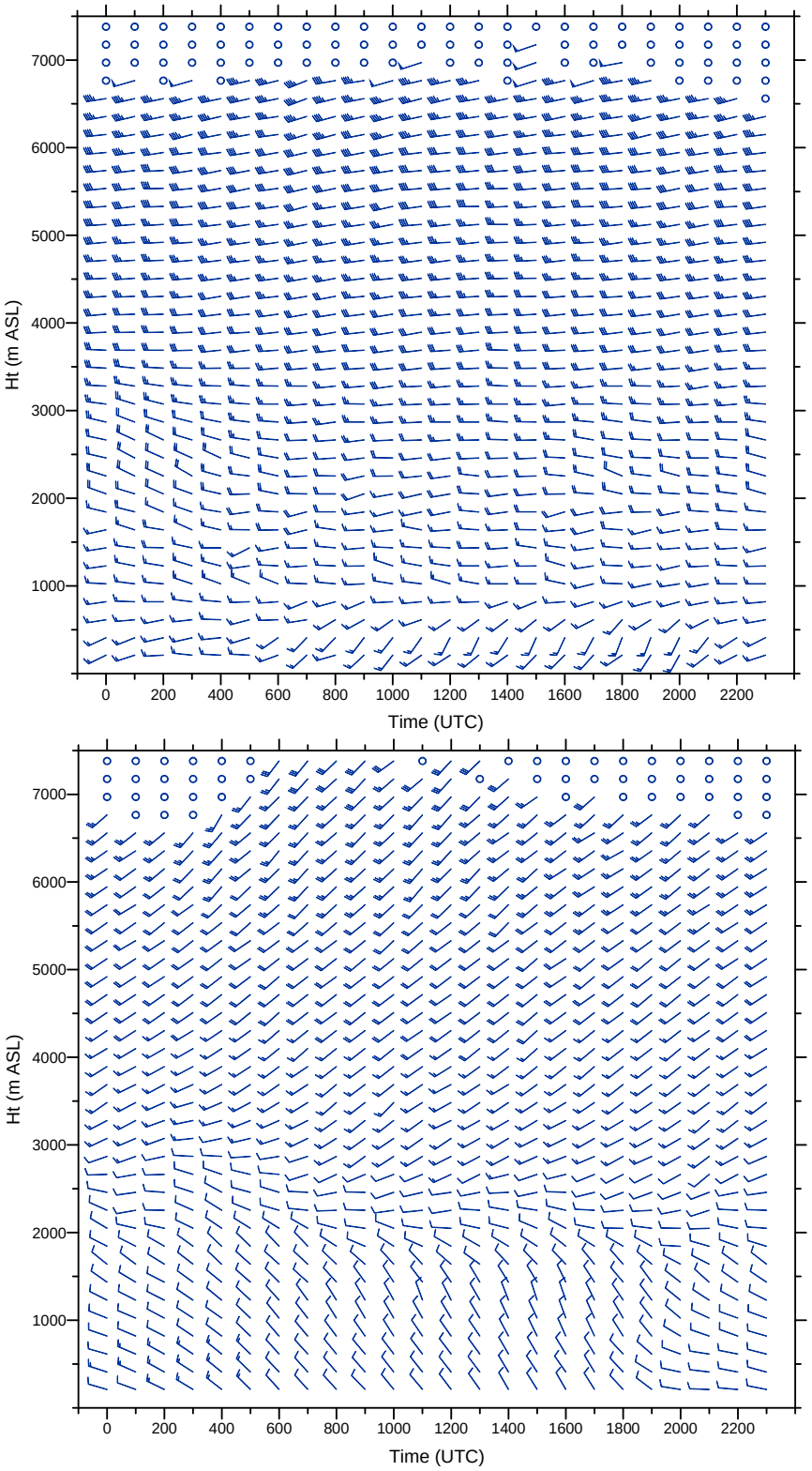

Figure 3.1-2 Diurnal composites of BBY 449-MHz wind profiles from the high mode for the winter (top) and summer (bottom) seasons. Wind barbs as in Fig. 3.1-1.

BBY 915-MHz profiler winds: The results of the analysis are summarized in Table 3.1-2. The average height coverage for all data was 1861 m for the low mode and 2243 m for the high mode. For the high mode, the greatest height coverage occurred during the spring season with the least coverage during the winter. Figure 3.1-3 shows the diurnal composite of BBY 915-MHz profiler winds for the entire evaluation. Below 1400 m more than 90% of the available data were valid winds. The availability of valid winds drops off linearly between 1400 and 2300 m. Wind barbs show no diurnal variation in height coverage. Figure 3.1-4 shows the ensemble average of BBY winds for the winter and summer seasons. Height coverage during the summer months exceeds that obtained during the winter by 200 m.

Table 3.1-2 Bodega Bay 915-MHz wind profiler maximum height coverage statistics.

	Fall	*Winter*	*Spring*	*Summer*	*All data*
Low mode					
Mean height (m)	1829	1708	1999	1901	1861
Standard deviation	133	102	124	72	62
High mode					
Mean height (m)	2229	2120	2369	2255	2243
Standard deviation	101	151	102	89	64

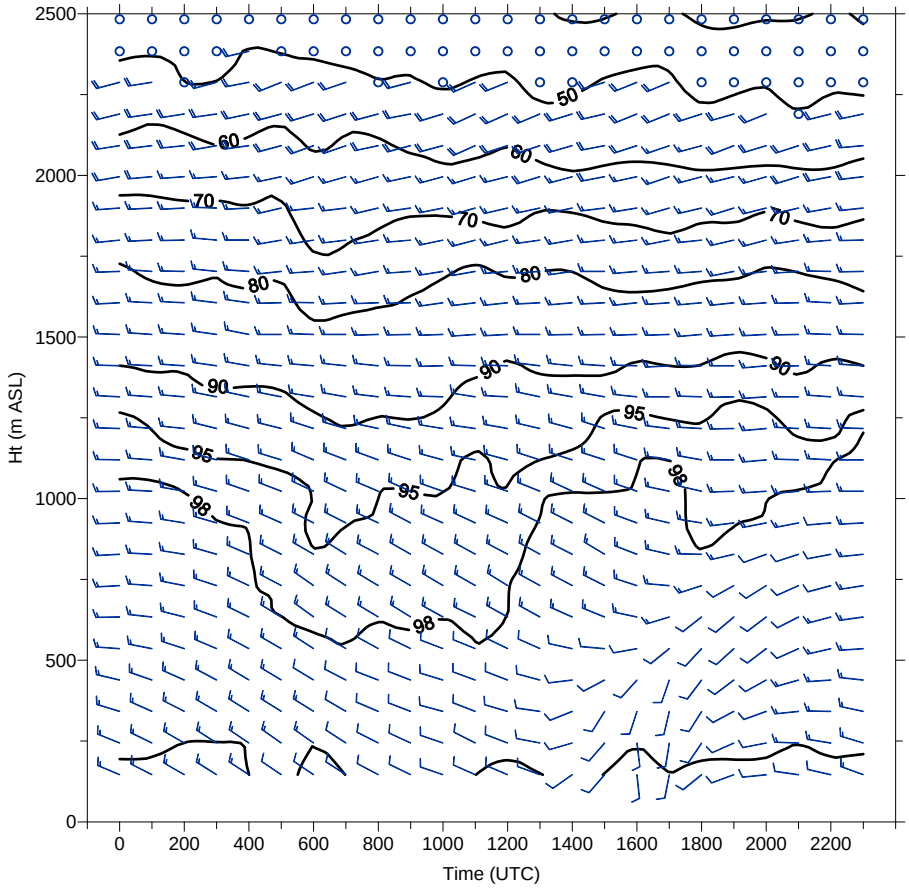

Figure 3.1-3 Diurnal composite of BBY 915-MHz wind profiles from the high mode for the entire evaluation. Contours and wind barbs as in Fig. 3.1-1..

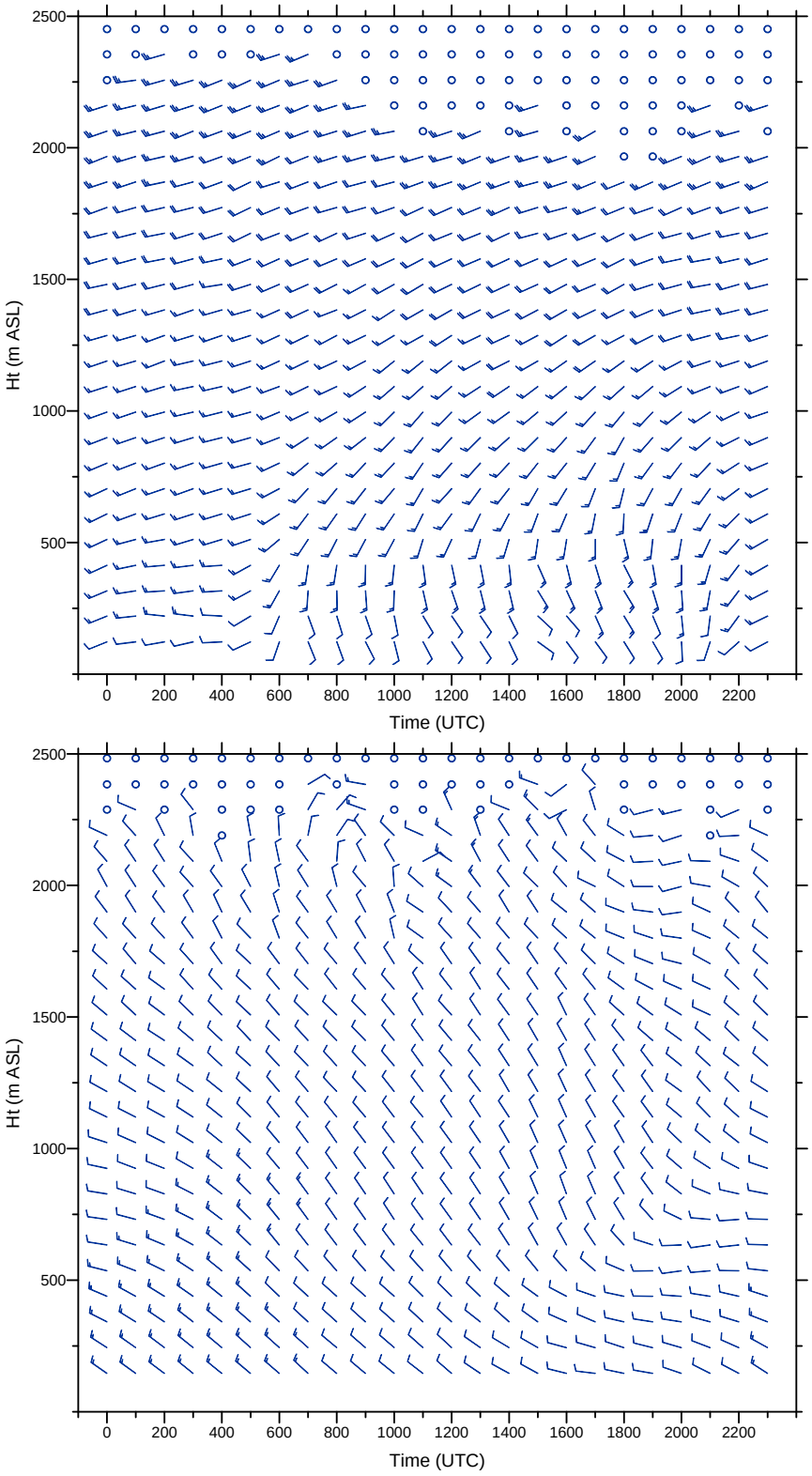

Figure 3.1-4 Diurnal composites of BBY 915-MHz wind profiles from the high mode for the winter (top) and summer (bottom) seasons. Wind barbs as in Fig. 3.1-1.

Comparison between BBY 915-MHz and 449-MHz profiler winds: The results of the comparison are summarized in Table 3.1-3. For the entire data set, the 449-MHz profiler maximum height coverage exceeds that obtained by the 915-MHz profiler by more than 4600 m. The advantages of the 915-MHz profiler are the higher resolution in approximately the lowest 2000 m and the lower minimum height (122 m vs. 197 m). The advantage of the 449-MHz profiler is a maximum height coverage that exceeds that of the 915-MHz profiler by more than a factor of three.

Table 3.1-3 BBY 449-MHz and 915-MHz wind profiler maximum height coverage statistics.

	Fall	*Winter*	*Spring*	*Summer*	*All data*
449-MHz high mode					
Mean height (m)	7111	6734	6760	6922	6845
915-MHz high mode					
Mean height (m)	2229	2120	2369	2255	2243
Difference (m)	4882	4614	4391	4667	4602

GLA 449-MHz profiler winds: The results of the analysis are summarized in Table 2.4. The average height coverage for all data was 4451 m for the low mode and just less than 6000 m for the high mode. For the high mode, the greatest height coverage occurred during the fall with the least coverage during the summer. Figure 3.1-5 shows a diurnal composite of GLA 449-MHz profiler winds for the entire evaluation. Below 4500 m more than 90% of the available data were valid winds. The availability of valid winds drops off sharply between 4500 and 5500 m and linearly above 5500 m. The sharp drop off of available data around 5000 m is an artifact of the ground clutter removal algorithm used at GLA. Approximately 5 km north of the site, the Santa Ynez Mountains rise abruptly from the coastal plain to heights exceeding 1 km. During light wind conditions aloft (i.e. during the summer months), ground clutter from vegetation movement along the mountain slopes overwhelms the atmospheric signal and biases the calculated winds towards zero. During these conditions, winds above 5000 m meeting a certain threshold are eliminated from the consensus average causing a sharp drop off of valid winds near the 5000-m level. Wind barbs show a distinct boundary layer structure in the lowest 2000 m with westerly flow dominating aloft. Wind barbs show no diurnal variation in height coverage. Figure 3.1-6 shows the diurnal composites of GLA profiler winds for the winter and summer seasons. The winter season exhibits the dominance of westerly flow aloft with some boundary layer structure in the lowest 1500 m. The summer season shows the influence of thermal and terrain forcing in the lowest 2000 to 3000 m with the prevailing southerlies aloft. Height coverage for the high mode during the summer was greatly reduced when compared to the other seasons because of the clutter removal algorithm.

Table 3.1-4 GLA 449-MHz wind profiler maximum height coverage statistics.

	Fall	*Winter*	*Spring*	*Summer*	*All data*
Low mode					
Mean height (m)	4541	4200	4183	4949	4451
Standard deviation	150	187	230	188	128
High mode					
Mean height (m)	6251	6020	6054	5472	5986
Standard deviation	222	313	313	210	185

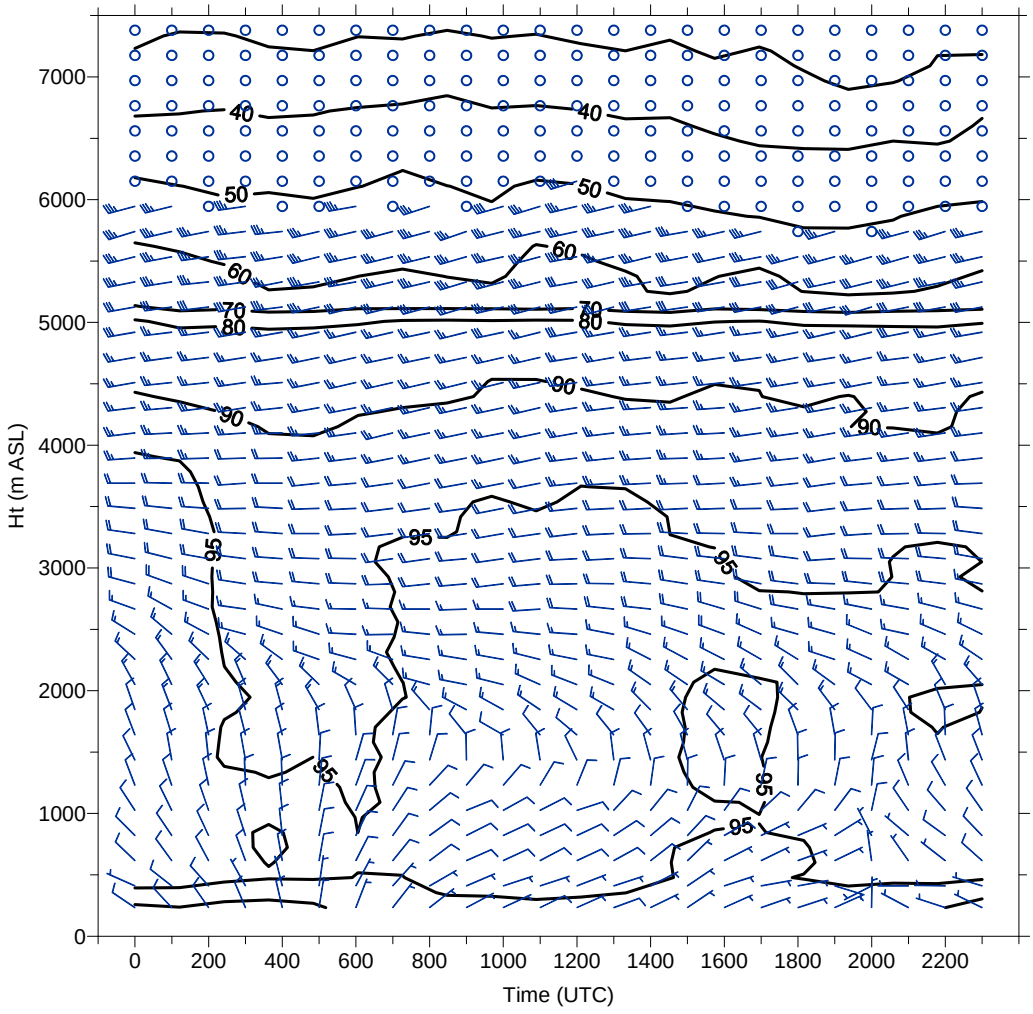

Figure 3.1-5 Diurnal composite of GLA 449-MHz wind profiles from the high mode. Contours indicate the percentage of valid data points used to obtain the composite for the entire evaluation. Contours and wind barbs as in Fig. 3.1-1.

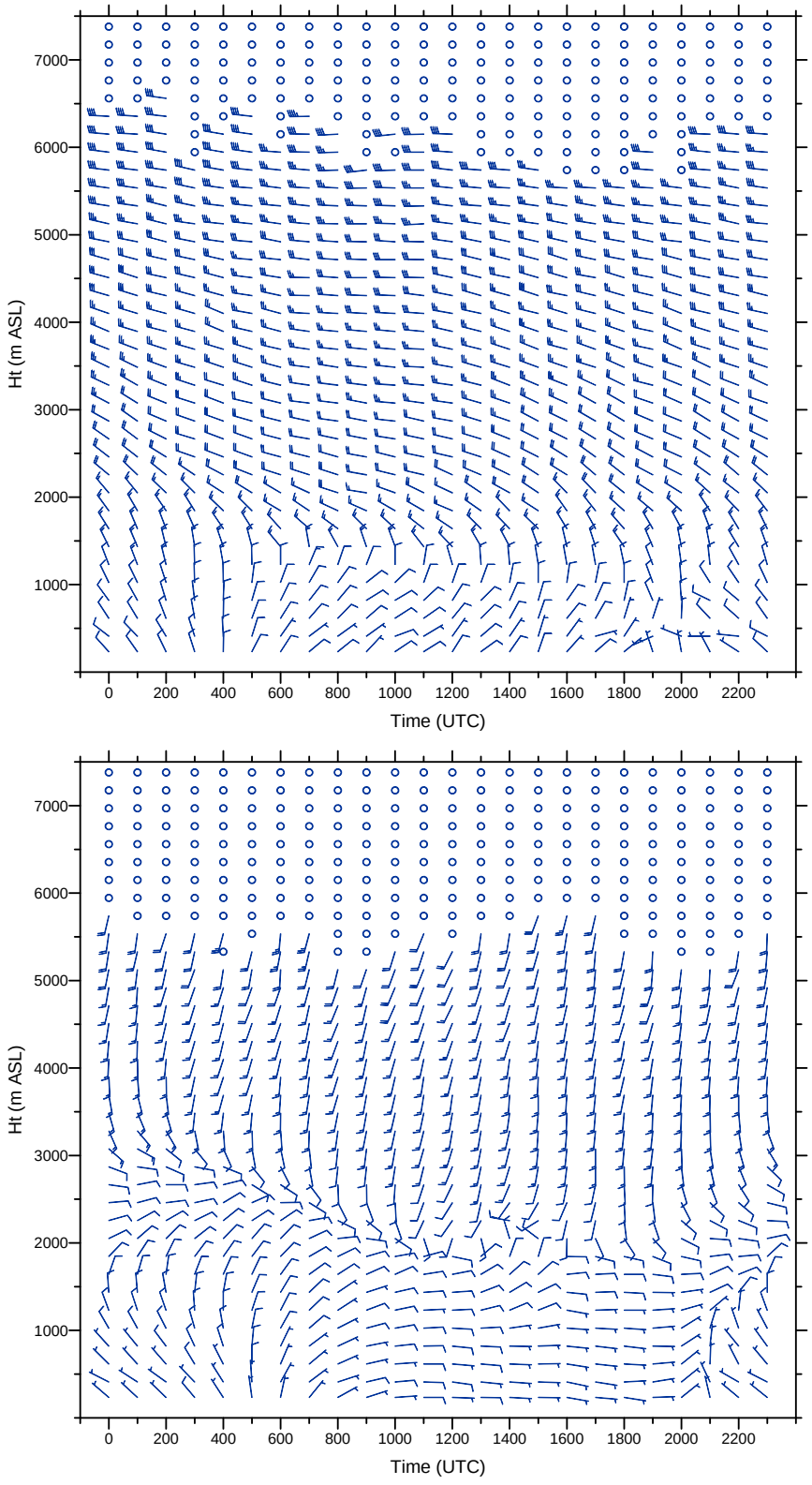

Figure 3.1-6 Diurnal composites of GLA 449-MHz wind profiles from the high mode for the winter (top) and summer (bottom) seasons. Wind barbs as in Fig. 3.1-1.

Comparison between BBY and GLA 449-MHz profiler winds: The results of the comparisons are summarized in Table 3.1-5. Bodega Bay maximum height coverage exceeded that at Goleta by an average of 859 m. It is unclear whether this difference is a result of dissimilarities in the refractive index fluctuations in the upper atmosphere above the sites or in the performance of the individual radars. However, the BBY site was equipped with a new transmitter and new antenna (supplied by Vaisala, Inc. for the evaluation) that could have contributed to the enhanced performance.

Table 3.1-5 BBY and GLA 449-MHz, high mode wind profiler maximum height coverage statistics.

Bodega Bay	Fall	Winter	Spring	Summer	All data
Mean height (m)	7111	6734	6760	6922	6845
Goleta					
Mean height (m)	6251	6020	6054	5472	5986
Difference (m)	860	714	706	1450	859

BBY 915-MHz RASS virtual temperatures: Results of the analysis are summarized in Table 3.1-6. Greater height coverage during the fall and winter months was a result of weaker winds in the lowest 1000 m of the atmosphere. The spring and summer months showed a weak diurnal pattern with the lowest coverage during the late afternoon and early evening hours, a result of stronger, thermally-driven flows during those time periods. RASS combines acoustic sources with wind profilers to measure the profile of virtual temperature (Peters et al. 1983). The wind profiler measures the speed of refractive index perturbations induced by the acoustic waves as they ascend in the atmosphere. Winds will bend the acoustic beam to a point where the acoustically induced signal becomes too weak to detect, thus stronger winds will result in lower height coverage.

Table 3.1-6 BBY 915-MHz RASS virtual temperature maximum height coverage statistics.

	Fall	Winter	Spring	Summer	All data
Mean height (m)	699	686	625	607	646
Standard deviation	32	27	24	37	36

GLA 915-MHz RASS virtual temperatures: Data obtained from September 15, 2001 to August 15, 2002 were used to provide a comparison with the 449-MHz RASS obtained during the IOOS technology evaluation. The results are summarized in Table 3.1-7. Figure 3.1-7 shows a diurnal composite of 915-MHz RASS virtual temperatures for the entire 11-month period. Maximum height coverage averaged just less than 1050 m. Figure 3.1-8 shows the ensemble average for the summer season. Both figures show the diurnal heating/cooling cycle and the presence of the marine inversion during the summer months but the measurements don't extend quite high enough to show the entire thermal structure of the boundary layer. Unlike at BBY, winds at GLA tend to be weak over the lowest 1000 m

during all times of the year, which helps to explain the increased maximum altitude coverage of the 915-MHz RASS at GLA as compared to the 915-MHz RASS at BBY. At GLA, the summer average maximum height coverage exceeded that of the winter by 220 m.

Table 3.1-7 GLA 915-MHz RASS virtual temperature maximum height coverage statistics.

	Fall	Winter	Spring	Summer	All data
Mean height (m)	955	937	1128	1157	1047
Standard deviation (m)	79	34	61	58	49

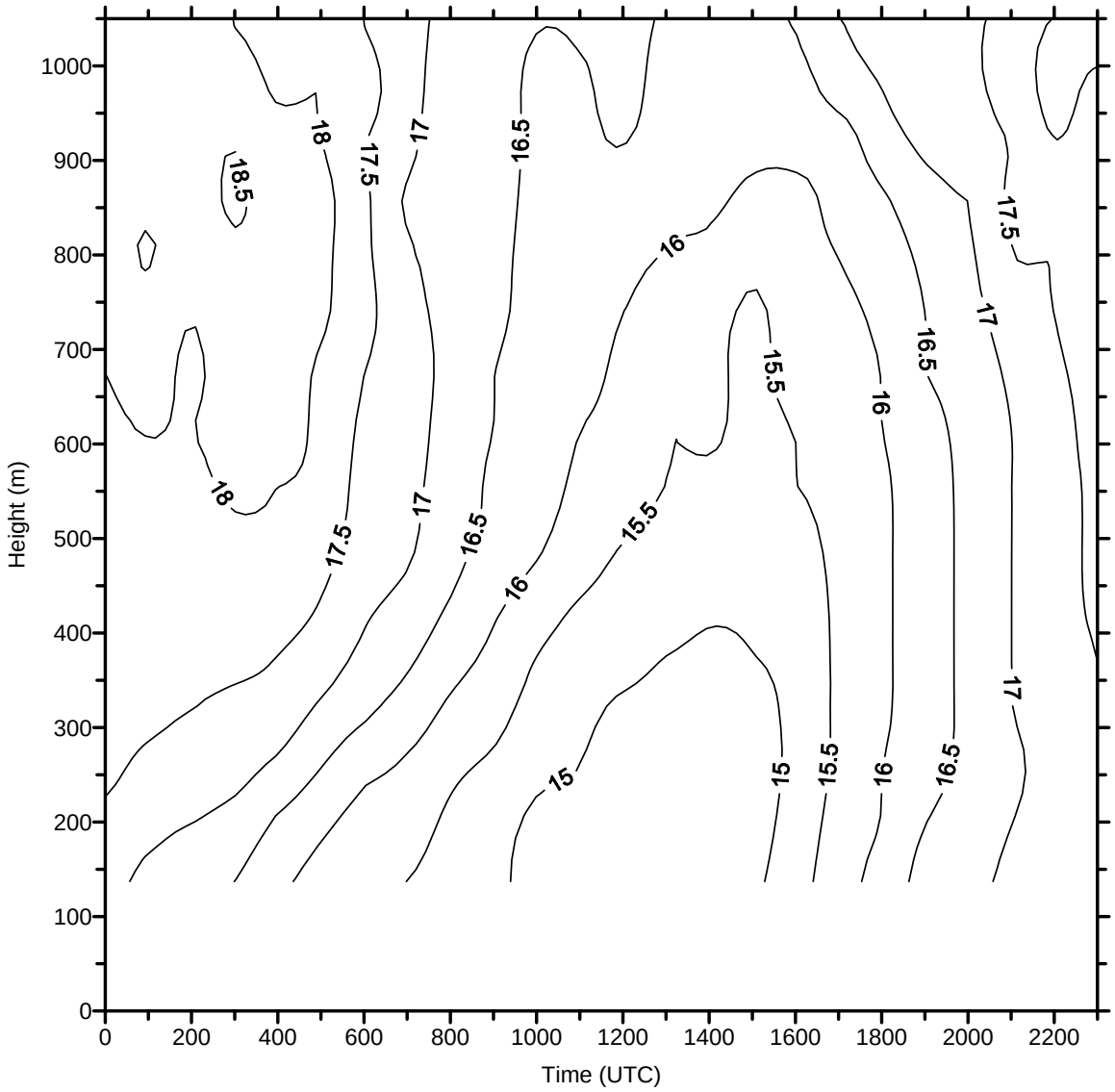

Figure 3.1-7 Diurnal composite of GLA 915-MHz RASS virtual temperatures (^{o}C) for the entire 11-month period in 2001-2002 that corresponds to the same 11-month IOOS measurement period in 2005-2006.

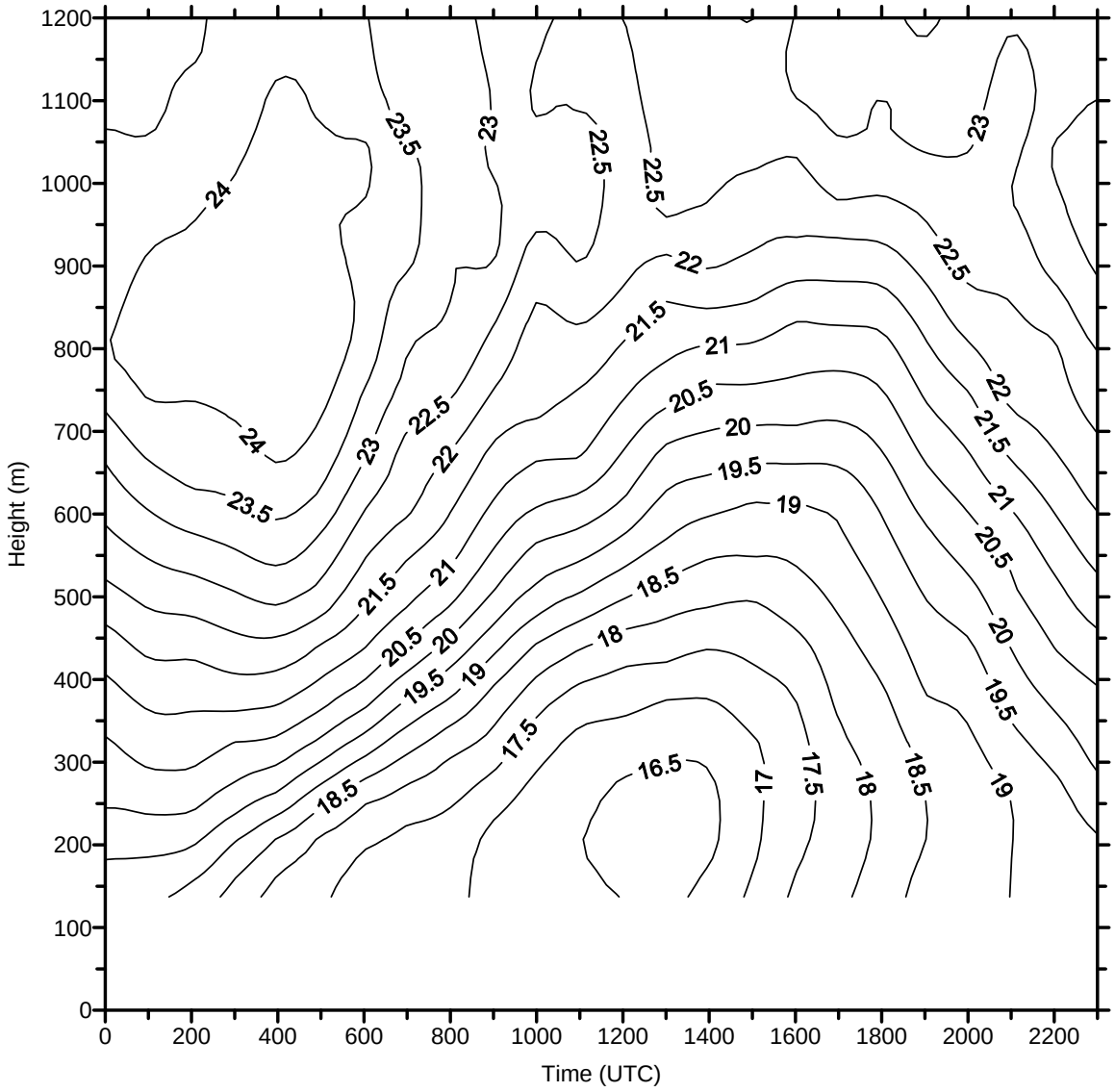

Figure 3.1-8 Diurnal composite of GLA 915-MHz RASS virtual temperatures (^{o}C) for the summer season of 2002.

GLA 449-MHz RASS virtual temperatures: Table 3.1-8 summarizes the virtual temperature maximum height coverage statistics. Figure 3.1-9 shows a diurnal composite of 449-MHz RASS virtual temperatures for the entire IOOS evaluation. Maximum height coverage averaged 1734 m and there was no evidence of a diurnal pattern in the height coverage. Figure 3.1-10 shows the ensemble average for the summer season. Both figures show the entire thermal structure of the boundary layer. Similar to the GLA 915-MHz RASS height coverage, the summer average maximum height coverage for GLA 449-MHz RASS exceeded that of the winter by more than 300 m.

Table 3.1-8 GLA 449-MHz RASS virtual temperature maximum height coverage statistics.

	Fall	Winter	Spring	Summer	All data
Mean height (m)	1703	1585	1809	1991	1734
Standard deviation	0	36	0	49	49

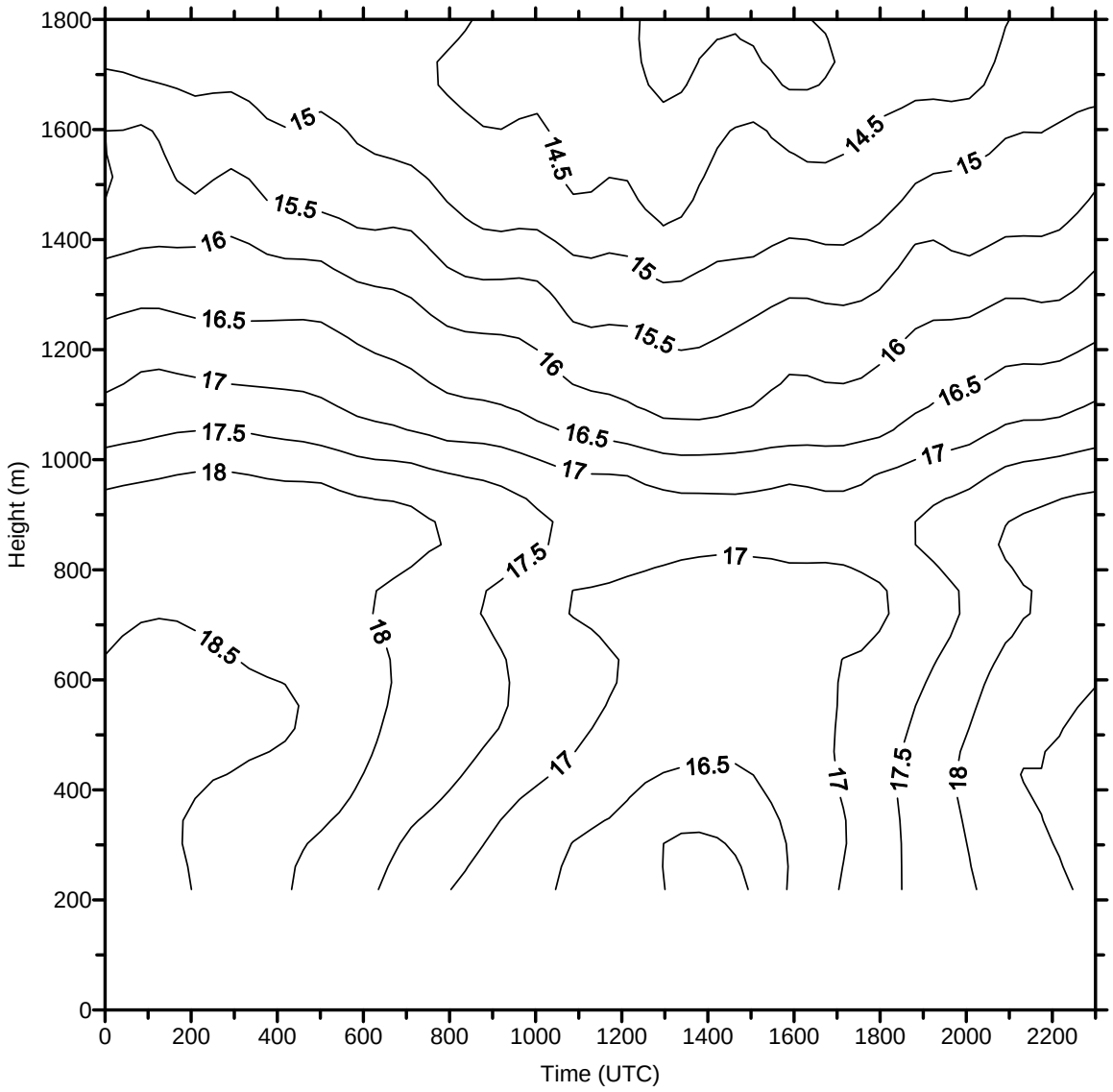

Figure 3.1-9 Diurnal composite of Goleta 449-MHz RASS virtual temperatures (^{o}C) for the entire IOOS evaluation.

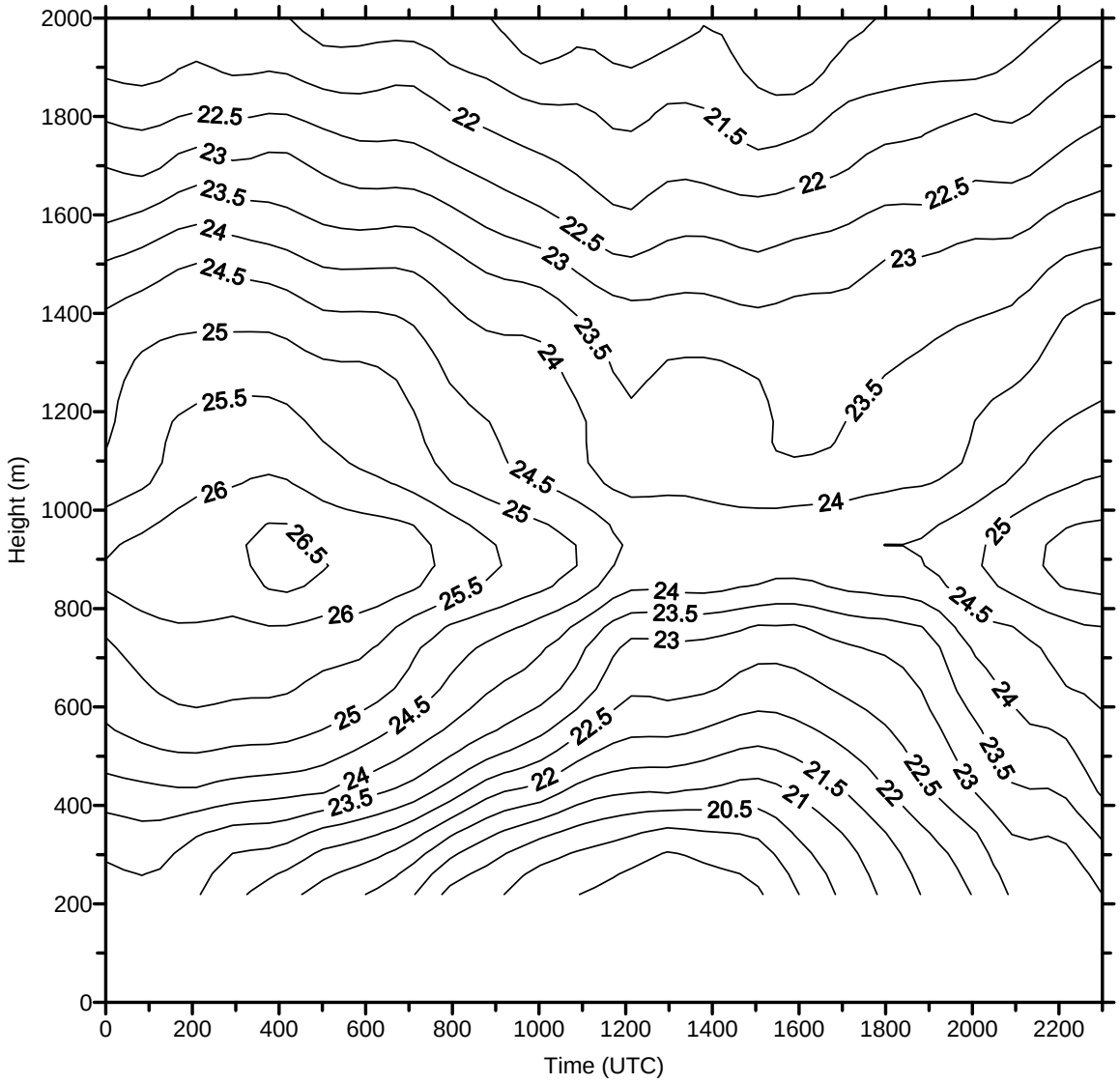

Figure 3.1-10 Diurnal composite of GLA 449-MHz RASS virtual temperatures (^{o}C) for the summer season.

Comparison between GLA 915-MHz and 449-MHz RASS virtual temperatures: Although a direct comparison is not available because the datasets were collected during different years, the following results still show the relative difference in performance of the two RASS systems for the same 11-month period. The results of the comparison are summarized in Table 3.1-9. For the entire 11-month corresponding periods, the 449-MHz maximum height coverage exceeds that obtained by the 915-MHz system by close to 700 m. The advantages of the 915-MHz RASS are the higher resolution (60 m vs. 106 m) in approximately the lowest 1000 m and the lower minimum height (152 m vs. 219 m). The advantage of the 449-MHz RASS is its maximum height coverage that exceeds that of the 915-MHz RASS by nearly 700 m allowing for the measurement of virtual temperatures throughout the boundary layer.

Table 3.1-9 GLA 449-MHz and 915-MHz RASS virtual temperature maximum height coverage statistics.

	Fall	*Winter*	*Spring*	*Summer*	*All data*
449-MHz RASS					
Mean height (m)	1703	1585	1809	1991	1734
915-MHz RASS					
Mean height (m)	955	937	1128	1157	1047
Difference (m)	748	648	681	834	687

4.0 Detection, Monitoring, and Uses for Select, Key Coastal Weather Phenomena

In this section, data from the ¼-scale 449-MHz and 915-MHz wind profilers are compared with respect to how well they were able to detect and monitor important processes or variables associated with coastal and marine weather prediction. The list here is not an exhaustive catalog of demonstrated wind profiler applications, but these analyses provide an additional way to evaluate the relative performance of the two profiler technologies and illustrate a few examples of how the data might be used operationally.

4.1 Gap Flow

Mountains can profoundly modify stably stratified, lower-tropospheric air streams, resulting in shallow and relatively cold blocked flows trapped against the high terrain. Blocking deflects the low-level flow upstream and below the top of mountain ranges (e.g., Bell and Bosart 1988; Colle and Mass 1995) and results in the formation of a barrier jet below mountain top that parallels the long axis of quasi-two-dimensional high terrain (e.g., Parish 1982; Marwitz 1983; Overland and Bond 1995; Doyle 1997). It can also locally redistribute precipitation, inhibit the forward motion of approaching fronts, and produce strong winds due to the superposition of a barrier jet and prefrontal low-level jet (LLJ) (e.g., Dunn 1987; Peterson et al. 1991; Marwitz and Toth 1993; Doyle 1997; Sinclair et al. 1997; Braun et al. 1999; Doyle and Bond 2001; Yu and Smull 2000; Yu and Bond 2002; Neiman et al. 2002 and 2004; Medina and Houze 2003).

A host of physical mechanisms can contribute to the generation of shallow, stably stratified air trapped along the California coast during the cool season. For example, a remnant cold pool can remain trapped against the mountains following the passage of a warm front aloft (e.g., Bjerknes and Solberg 1921; Garner 1999). Orographically forced ascent of a stably stratified air stream yields a dome of adiabatically cooled air and windward ridging (e.g., Smith 1979). Diabatic cooling via evaporation of rainfall in subsaturated conditions provides an effective mechanism for creating shallow pooling of cold air (e.g., Carbone et al. 1995; Wang and Chen 1998). The melting of hydrometeors offers another diabatic process by which shallow cold air can be created (e.g., Marwitz and Toth 1993; Bousquet and Smull 2003; Steiner et al. 2003). Another mechanism, which is the focus of this section, is the extrusion or channeling of cold continental air through gaps in mountainous terrain. Gap flows can act as a source of cold, dry air, especially in temperate coastal zones (e.g., Overland and Walter 1981; Bond et al. 1997; Loescher et al. 2006; Colle et al. 2006), California among them.

During winter, channeled air streams regularly exit California's Central Valley to the coast through its only major airshed outlet, the Petaluma Gap (Fig. 4.1-1; from Neiman et al. 2006). These wintertime gap flows are generally less pronounced than those observed farther north [i.e., in the Pacific Northwest (e.g., Colle and Mass 2000; Sharp 2002), British Columbia (e.g., Mass et al. 1995; Jackson and Steyn 1994), and Alaska (e.g., Bond and Stabeno 1998; Loescher et al 2006; Colman and Dierking 1992)], in part because the Petaluma Gap is poorly defined by comparison (~35-50 km wide, and walls extending a modest 600-900 m above the valley floor – see Fig. 1b). Petaluma Gap flows are also

weaker because the source of cold air is California's Central Valley rather than the northern interior of North America where arctic air is ubiquitous. Specifically, the Sierra Nevada Mountains act as a continuous 3-4 km tall barrier that prevents very cold air in the continent's interior from regularly entering the Central Valley. Rather, cold air in the Central Valley usually forms in-situ when air within the valley stagnates beneath a capping subsidence inversion and radiatively cools for an extended period of time, often producing widespread fog or stratus which inhibits diurnal heating (e.g., Gilliam 1970; Holets and Swanson 1981; Underwood et al. 2004). Nocturnal katabatic flows from the Sierras can also contribute to the generation and maintenance of the cold pool.

Despite the comparatively weak character of flows though the Petaluma Gap relative to their northern counterparts, these flows can significantly impact the local distributions of wind, temperature, precipitation, and atmospheric pollutants along the coast, as has been documented in detail in a five-winter wind profiler study by Neiman et al. (2006). Channeled flows exiting the Petaluma Gap preferentially occur in pre-cold-frontal conditions, largely because sea-level pressure decreases westward along the gap in a stably stratified atmosphere in advance of approaching cold-frontal pressure troughs. These flows are only several hundred meters deep and characterized by relatively cold, easterly flow capped by a layer of enhanced static stability and directional vertical wind shear. They can contribute to coastally trapped air streams in California, as has also been found in the coastal zone of Alaska by Loescher et al. (2006) and Colle et al. (2006).

Given the importance of channeled flows exiting the Petaluma Gap to regional weather, we deemed it instructive to take advantage of this shallow, terrain-anchored phenomenon to explore the capabilities and limitations of the ¼-scale 449-MHz wind profiler at BBY during the winter of 2005-2006. The basic analysis methodology employed for this study was the same as that in Neiman et al. (2006). Namely, we defined gap-flow events based on quality-controlled 915-MHz wind profiler data (Section 2.3) and surface observations at BBY meeting the following criteria for at least six consecutive hours: (1) a surface wind direction of 50-120 degrees, (2) a layer-mean wind direction of 60-130 degrees between 100-350 m MSL (i.e., in the lowest three profiler range gates), and (3) an easterly component of at least 5 m s^{-1} in the same 100-350 m layer. A total of 19 gap-flow events were observed between 1 November 2005 and 26 April 2006 (Table 4.1-1).

The 19 gap-flow events (Table 4.1-1) ranged between 6 and 41 h in duration, with a mean time interval of ~14 h. Each case exhibited an above-surface maximum of low-level easterly-component flow (hereinafter referred to as a gap jet) beneath the top of the gap walls, with the mean altitude of this maximum residing at 306 m MSL. The mean magnitude of the gap jet was 8.9 m s^{-1} and was bounded by cases as strong as 13.1 m s^{-1} and as weak as 6.0 m s^{-1}. Most of the 19 cases were rain-free, thus supporting the conclusions drawn from the 5-winter study by Neiman et al. (2006) that gap-flow events inhibit rainfall near its exit at the coast. In addition, without exception, the summary gap-flow statistics based on the analysis of the 2005-2006 profiler data mirror those of the 5-winter study. Hence, the gap flow characteristics observed at BBY during the winter of 2005-2006 should be deemed representative.

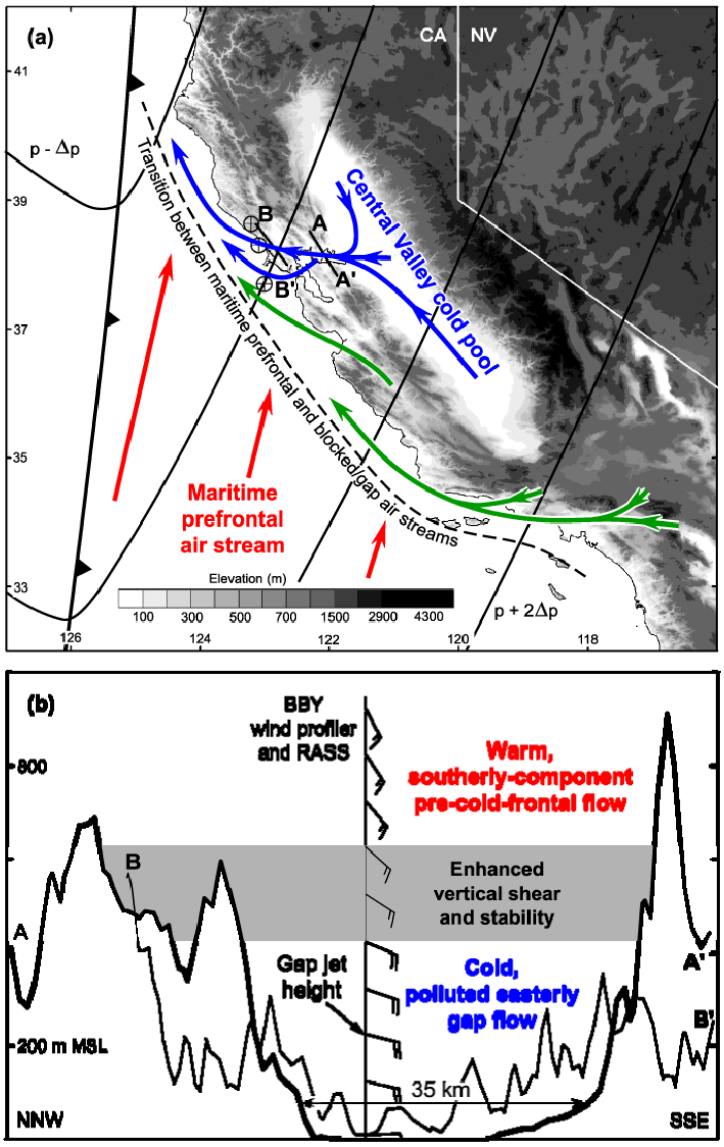

Figure 4.1-1 Summary results based on a recent five-winter study by Neiman et al. (2006). (a) Plan view conceptual representation of cold, dry gap flow at the surface originating from California's Central Valley (solid blue) and exiting the Petaluma Gap near the BBY profiler (the middle circular symbol along the coast) and the Golden Gate Gap near San Francisco. Gap flow is also shown exiting the interior farther to the south (green lines). A warm maritime prefrontal air stream is portrayed (red) ahead of an advancing cold front. Solid black lines are isobars, and the dashed black line marks the transition between the prefrontal and blocked/gap air streams. Bold lines AA' and BB' are cross-section projections across the Petaluma Gap in (b). Terrain is shaded (see key). (b) Schematic terrain cross sections along AA' and BB' highlighting the key kinematic and thermodynamic attributes of shallow, easterly flow through the Petaluma Gap, based on composite wind profiles from BBY (barbs = 5 m s^{-1}; half-barbs = 2.5 m s^{-1}) and collocated RASS observations.

Table 4.1-1 Gap-flow case inventory (19 total) and gap jet characteristics based on quality-controlled 915-MHz wind profiler data at BBY between 1 Nov 2005 and 26 Apr 2006. Rainfall at BBY is also shown. Summary statistics from the five-winter gap flow wind profiler study between November 1997 and March 2004 by Neiman et al. (2006) are provided at the bottom.

Start date/time	Hours	Gap flow jet. Altitude of max. easterly flow (m, MSL)	Gap flow jet. Magnitude of max. easterly flow ($m\ s^{-1}$)	Gap flow jet. Wind dir. in max. easterly flow (deg)	Rainfall at BBY (mm)
16Nov05 08Z	12	512	9.0	93.3	0.0
18Nov05 13Z	9	317	9.2	86.3	0.0
28Nov05 21Z	9	221	9.0	115.4	19.558
30Nov05 15Z	11	221	7.7	108.4	0.0
07Dec05 22Z	17	317	7.5	102.5	0.508
18Dec05 02Z	9	317	13.1	121.3	35.052
24Dec05 00Z	24	317	9.2	103.0	0.254
04Jan06 12Z	6	221	7.9	111.1	0.508
04Jan06 22Z	41	221	10.3	106.3	0.0
13Jan06 03Z	17	221	9.2	108.9	0.0
24Jan06 16Z	10	317	8.4	99.0	0.0
06Feb06 06Z	34	317	9.7	94.5	0.0
09Feb06 07Z	17	317	10.4	88.1	0.0
19Feb06 05Z	8	512	8.2	77.8	0.0
15Mar06 05Z	6	317	6.0	127.2	0.508
21Mar06 12Z	6	317	7.8	104.0	0.0
02Apr06 15Z	14	342	8.5	120.2	12.700
04Apr06 10Z	11	244	10.3	103.4	3.556
12Apr06 18Z	9	244	8.1	109.5	2.286
Total	270				74.93
Mean (all)	14.2	305.9	8.9	104.2	3.944
Standard Dev.	9.5	85.3	1.5	12.6	9.115
Minimum	6	221	6.0	77.8	0.0
Maximum	41	512	13.1	127.2	35.052
5-y study Total	937				57.404
Mean (all)	15.1	226.4	9.1	104.8	0.926
Standard Dev.	13.3	113.0	1.9	14.5	2.567
Minimum	6.0	105.0	6.0	66.4	0.0
Maximum	73.0	741.0	16.2	139.1	10.668

The mean vertical structure of the flow through (and above) the Petaluma Gap was evaluated by averaging all 270 hourly, quality-controlled wind profiles from the 19 gap flow cases into composite profiles of total wind speed, wind direction, and zonal and meridional wind components (dark blue curves in Fig. 4.1-2 a-d). The number of data points available at each range gate (a maximum of 270 for the winter of 2005-2006 versus 937 for the five-winter study) is shown in Figs. 4.1-2 e,f. The composite wind speed and direction profiles portray a gap jet (9.5 ± 2.5 m s^{-1}) directed from the east-southeast (i.e., from the Petaluma Gap) centered on the third range gate (i.e., at ~300 m MSL). The magnitude of the flow decreases significantly across a prominent directional shear layer at ~0.5 km MSL[2] and remains weaker than the gap jet upward through 2 km MSL. Clockwise turning of winds with height from southeasterly to southerly above the gap flow suggests the presence of pre-cold-frontal warm

[2] The altitude of this shear layer approximately coincides with the top of shallow cold air exiting the gap in two case studies presented in Neiman et al. (2006). It also generally matches the mean depth of the cold air trapped in the Central Valley during the long-lived Central Valley cold-pool event summarized in Fig 2 of Neiman et al. (2006).

advection, consistent with the findings in Neiman et al. (2006). Inspection of the composite zonal wind profile reveals a well-defined easterly gap-jet signature (9.2 $\pm$ 2.3 m s^{-1}), also at the third range gate. In contrast, the meridional wind profile shows a steady increase with height of the magnitude of the southerly component flow (from nearly zero to more than 8 m s^{-1}) in the lowest 1.5 km MSL. These composite profiles are remarkably similar to those based on the five-winter study (dashed curves in Figs. 4.1-2 a-d), although the altitude of the gap jet was slightly higher (by less than 100 m) during the winter of 2005-2006. These composite profiles also mirror their counterparts derived from the realtime 915- and 449-MHz profiler data during the winter of 2005-2006 (light blue and yellow curves in Figs. 4.1-2 a-d), with the notable exception that the gap jet resided in the two lowest range gates of the 449-MHz profiler (i.e., at ~200-300 m MSL).

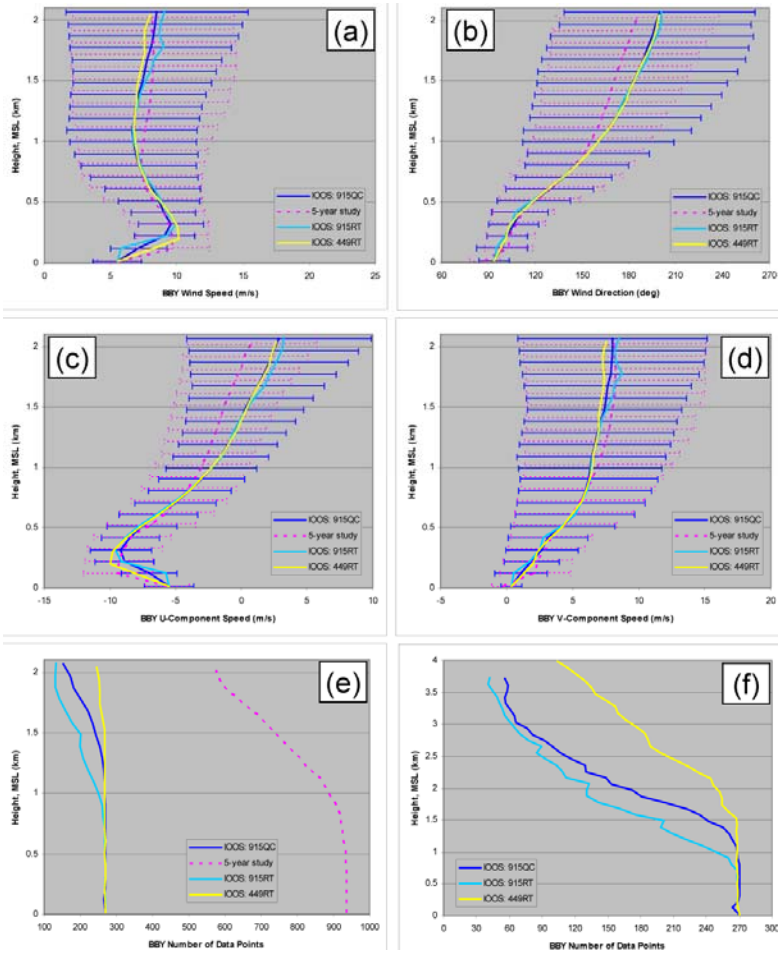

Figure 4.1-2 Composite mean profiles from the BBY wind profilers based on all 19 gap-flow cases observed during the winter of 2005-2006 (solid curves; dark blue = 915 MHz quality-controlled data, light blue = realtime data, yellow = realtime 449 MHz data). Composite mean profiles based on the 5-winter, 62-case study by Neiman et al. (2006) are also shown (dashed curves). (a) wind speed (m s^{-1}), (b) wind direction (deg), (c) U-component (i.e., zonal) wind speed (m s^{-1}), (d) V-component (i.e., meridional) wind speed (m s^{-1}), (e) number of hourly points per range gate, and (f) number of hourly points per range gate up to 4 km MSL for the current datasets only.

4.2 Melting Layer

The melting layer is the vertical layer of the atmosphere in which frozen hydrometeors transform into liquid hydrometeors during precipitation. The presence and location of the melting layer serves as important information for weather forecasters, hydrologists, water-resource managers, and emergency managers to asses or address rain/snow levels, water-management operations, and flooding issues.

The use of wind profilers offers an innovative approach to continuously monitor the melting layer during precipitation events. The Rayleigh scattering process, which has a strong inverse dependence on the wavelength of radiation being scattered, allows wind profilers in the UHF frequency band to detect hydrometeors in addition to the atmospheric turbulence that provides backscatter for clear-air wind profiling. Hydrometeors existing within the melting layer further alter the vertical profile of radar reflectivity, owing to the aggregation and water coating of snow flakes in the upper region of the layer and the mass flux divergence of rain drops in the lower region of the layer (Batton, 1973). These processes within the melting layer produce a peak in the radar reflectivity, which is referred to as the radar bright band (hereafter referred to RBB). NOAA has been detecting the RBB in real time on many of its remotely operated wind profilers since 2002. These data have been visualized and made accessible to NWS forecasters and the public through web interfaces in near-real time. An example of this product is shown in Fig. 4.2-1.

Both the 915-MHz and 449-MHz wind profilers are capable of detecting precipitation and the RBB. When considering radar wavelength alone, the shorter wavelength of the 915-MHz profiler (33 cm) makes it more sensitive for detecting the RBB than the 449-MHz profiler (67 cm). However, the 449-MHz wind profiler uses a low-noise receiver and a larger antenna than the 915-MHz wind profiler, which more than compensates for the sensitivity difference due to wavelength. The larger antenna allows for more scattered energy to be received, while the low-noise receiver produces signals with higher signal-to-noise ratios in the Doppler spectrum that are more easily detected by signal-processing algorithms. As depicted in Fig. 4.2-2, the combined effect of these hardware features makes the 449-MHz profiler more sensitive for detecting precipitation than the 915-MHz profiler. However, because the 449-MHz wind profiler is also able to detect much weaker levels of atmospheric turbulence than the 915-MHz wind profiler (also shown in Fig. 4.2-2), there is a much greater likelihood for two signal peak regions to exist in the 449-MHz Doppler spectra during precipitation – one from hydrometeors and another from the atmosphere. This scenario poses an additional challenge for signal-processing algorithms to select the desired signal associated with the RBB.

In an effort to quantify how these radar-hardware differences translate into differences in relative accuracy and data retrieval, comparisons were made between the derived bright-band heights for each radar data set. Using the technique described in White et al. (2002), the bright-band height was derived and averaged into hourly values for both radar data sets during the period October 25, 2005 – May 31, 2006. Because this technique uses bulk vertical gradients in reflectivity and radial velocity to identify the RBB, which typically varies between 300 m and 700 m in depth, vertical radar-range resolutions of approximately 100 m or less are required to adequately resolve these gradient features. During the IOOS

experiment, the sampling strategies for both radars were optimized for wind-profiling retrievals, with 63-m and 106-m modes for the 915-MHz profiler, and 106-m and 212-m modes for the 449-MHz profiler. The 63-m mode was used to better resolve lower elevation winds (below ~ 2 km), and the 212-m mode was used to detect higher elevation winds (5–10 km). For the purpose of bright-band detection, only the 63-m and 106-m modes were used. As a result, greater data-retrieval rates were obtained for the 915-MHz profiler because the shorter pulses used for its operating modes allowed for shorter sampling periods.

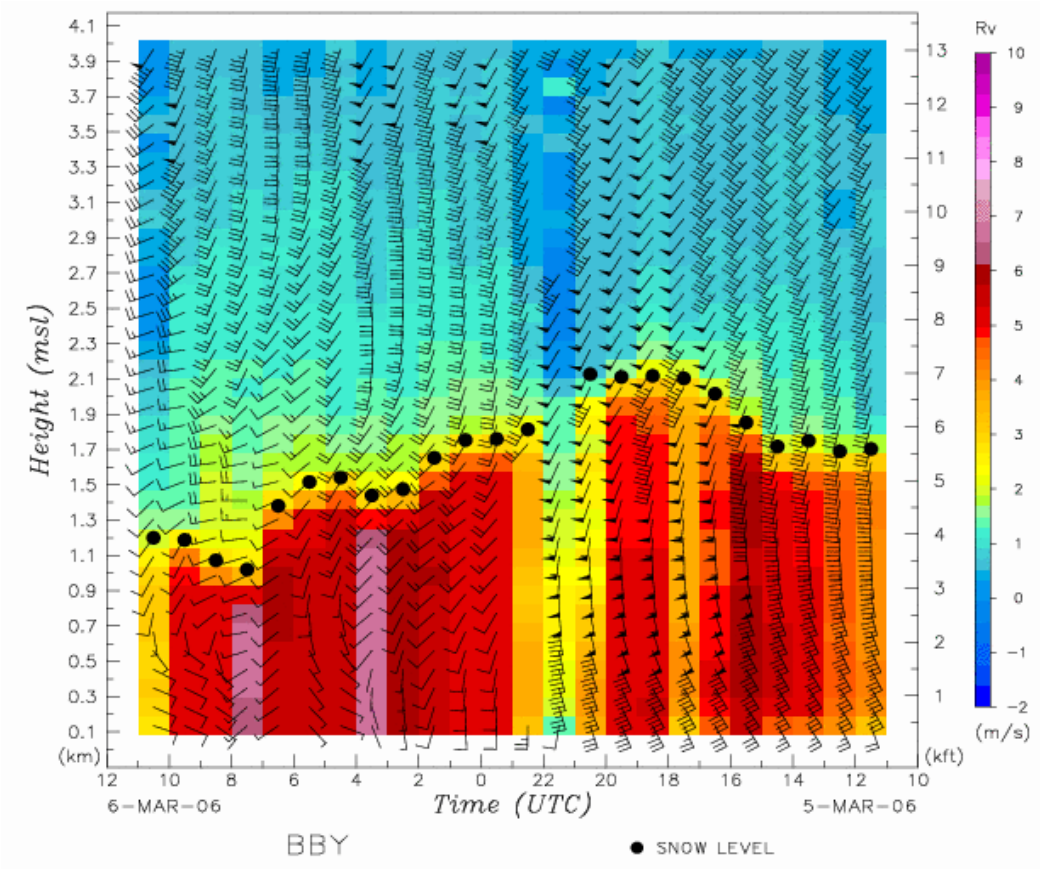

Time (UTC)	1030	0930	0830	0730	0630	0530	0430	0330	0230	0130	0030	2330
Snow Level (m)	1200	1188	1072	1020	1381	1516	1541	1440	1475	1653	1754	1760
Snow Level (ft)	3935	3896	3516	3345	4529	4972	5054	4723	4837	5421	5753	5772
Sfc Temp (C)	6.72	6.90	7.20	7.61	8.38	8.32	8.47	8.92	9.32	9.58	9.77	10.22

Time (UTC)	2230	2130	2030	1930	1830	1730	1630	1530	1430	1330	1230	1130
Snow Level (m)	1814	none	2127	2111	2117	2103	2016	1853	1717	1750	1690	1703
Snow Level (ft)	5949	none	6976	6924	6943	6897	6612	6077	5631	5739	5543	5585
Sfc Temp (C)	10.64	10.78	10.85	10.84	10.61	10.53	10.33	10.37	10.52	10.51	10.57	10.86

Figure 4.2-1 An example of NOAA's near-real-time, web-based, snow-level product from the BBY 915-MHz wind profiler on March 5-6, 2006. The radar bright-band heights are represented by the black dots, and the hourly-averaged vertical radial velocities associated with the hydrometeor fall speeds are contoured in color. Time increases from right to left on the horizontal axis. The table, added at the request of NWS forecasters in the Western U.S., lists both the snow level and the surface temperature, numerically.

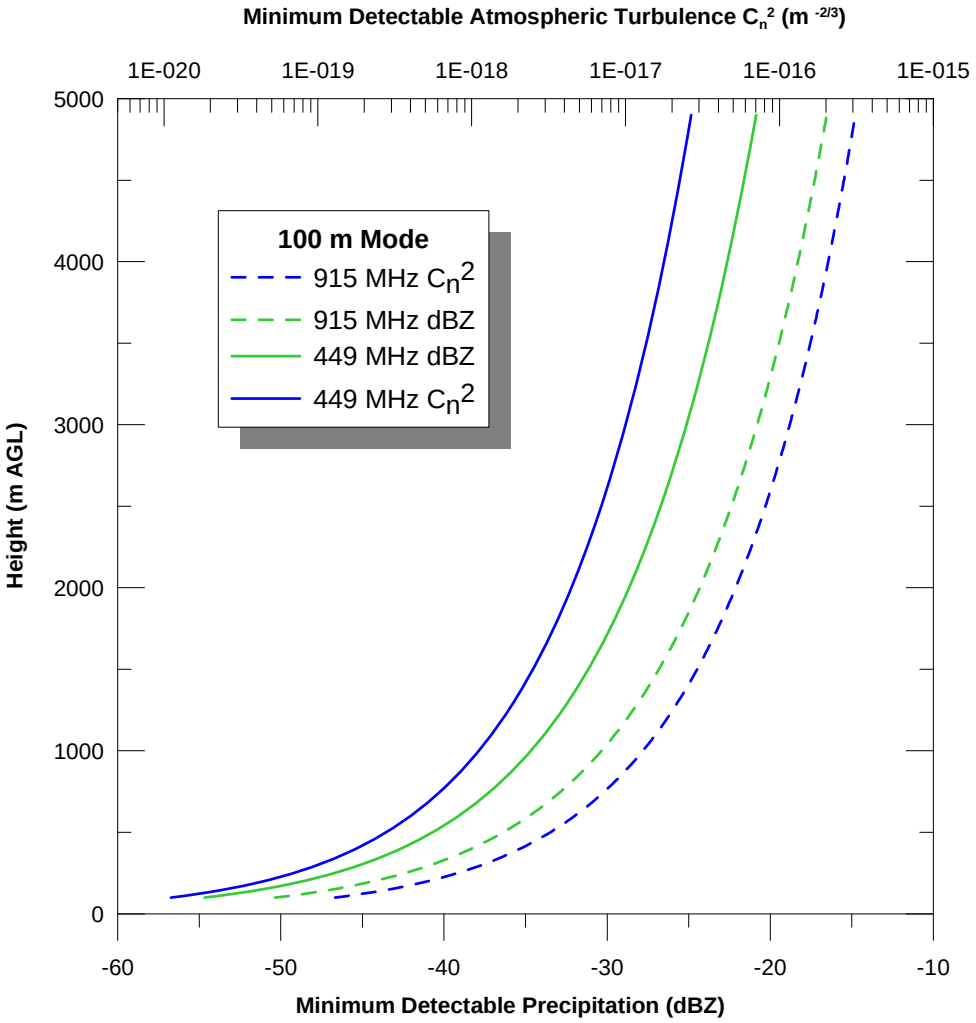

Figure 4.2-2 Vertical profiles of minimum detectable radar backscatter intensity, evaluated using the refractive index structure function parameter, C_n^2, and the effective radar reflectivity factor, dBZ, for the 106-m vertical resolution mode. The solid (dashed) lines correspond to the 449-MHz (915-MHz) wind profilers used in the technology evaluation.

Over the course of 66 days during the 218-day analysis period, a RBB was detected 322 times by both wind profilers during identical hours. The relative accuracy for these matched data was high, with a correlation coefficient of ~ 0.9993. With respect to data retrieval, the 915-MHz profiler detected 22% more RBBs than the 449-MHz profiler was able to detect, while the 449-MHz profiler detected only 3% more RBBs than the 915-MHz profiler was able to detect. This result is contrary to what might be expected, when considering the effect of radar sensitivity to precipitation alone (see Fig. 4.2-2).

The improved data-retrieval performance of the 915-MHz wind profiler is accounted for by two factors. First, as alluded to earlier, the utilization of both 915-MHz operating modes (i.e., the 63-m and 106-m modes) allows for more comprehensive temporal sampling during

the hour, and also produces a more statistically robust result by increasing the sample population for the bright-band detection algorithm. In addition, the higher vertical resolution of the 63-m mode provides a better approximation of the bulk gradients near and within the RBB. This is of particular importance for detecting RBBs that are shallow in depth or close to the earth's surface. This first factor accounts for 36% of the improved data-retrieval performance. The second and most prevalent factor results from the superior sensitivity of the 449-MHz profiler for detecting clear-air echoes attributable to atmospheric turbulence. This increased level of sensitivity allows signals from both the turbulence and precipitation to be resolved simultaneously in the 449-MHz Doppler spectrum. During light precipitation events, which correspond to lower values of radar reflectivity, the magnitude of the precipitation and turbulence echoes often can be nearly equivalent. This situation can pose a serious challenge for spectral-peak-picking algorithms to correctly and consistently identify precipitation signals for RBB detection. This was the case during several of the light- and intermittent-precipitation events encountered during the analysis period. It should be noted, however, that since the spectral peak-picking logic was originally developed for 915-MHz wind profilers, most of these 449-MHz dual-signal cases would likely be identified correctly with relatively minor enhancements to the algorithm.

Lastly, the impact of the additional data retrieved by the 915-MHz profiler was assessed. This impact was formulated in two ways. First, to what degree did the additional data aid in identifying the RBB for individual precipitation events? And, second, what type of association did these additional RBB data have with the precipitation rate observed at the surface? This targeted assessment may help determine to what degree the additional data provide beneficial information to the end user, such as weather forecasters or water-resource managers. In addressing the first question, 77% of the additional 915-MHz RBBs occurred during precipitation events that had at least one other RBB detected by the 449-MHz profiler during the event. Of these samples, a 449-MHz RBB was detected within +/- 2 hours of the 915-MHz RBB 72% of the time, with the remaining percentage occurring within +/- 3 to 7 hours. The remaining 33% of the additional 915-MHz RBBs occurred during events without a neighboring 449-MHz RBB during the event, and were all associated with intermittent precipitation events lasting 1 to 2 hours. The second question is addressed by reviewing the hourly accumulated precipitation, as acquired from a collocated surface rain gauge, during times when the additional RBBs were retrieved by the 915-MHz wind profiler. Figure 4.2-3 depicts the accumulated rainfall for all hours when a RBB was detected by both the 915-MHz and 449-MHz profilers (top panel), and for those hours when a RBB was only detected by the 915-MHz profiler (lower panel). The lower panel shows that most of the additional RBBs (97%) were associated with light precipitation regimes (accumulation less than or equal to 2 mm per hour). This result is consistent with the earlier explanation that the 449-MHz detection loss is associated with erroneously distinguishing light precipitation echoes from atmospheric turbulence echoes in the Doppler velocity spectrum. In addition, the hydrological consequences of excluding these additional RBBs, which are absent in the 449-MHz data set, are relatively low owing to their minimal contributions to rainfall runoff.

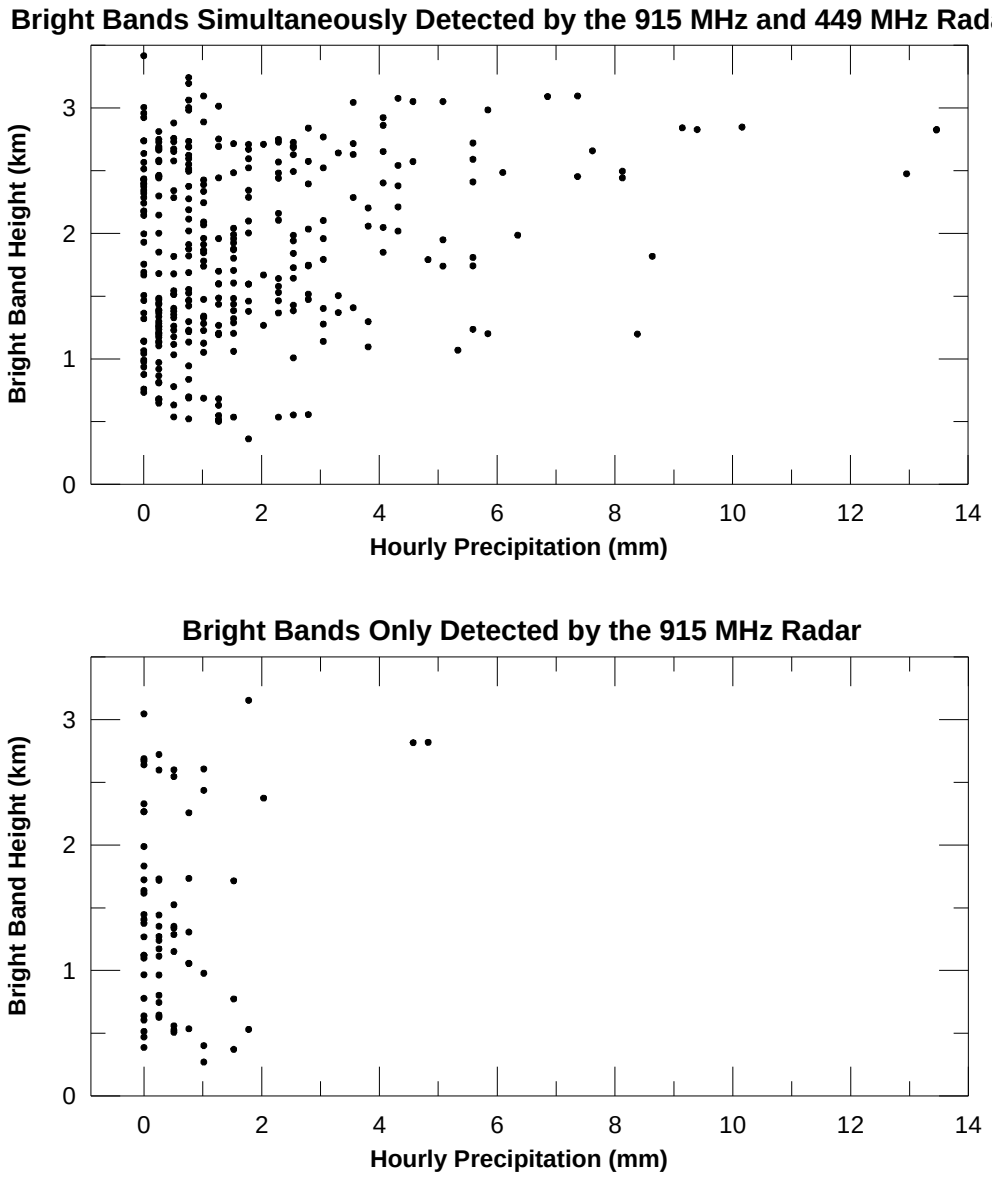

Figure 4.2-3 Hourly accumulated precipitation as a function of bright-band height for bright bands simultaneously detected by the 915-MHz and 449-MHz wind profilers (top panel) and for bright bands only detected by the 915-MHz wind profiler (bottom panel).

4.3 Boundary-layer Depth

The following analysis focuses on the estimation of the boundary-layer depth (BLD) using the data acquired by the wind profiling radars and RASS systems. At BBY, two profilers were operated, one at 449-MHz and one at 915-MHz. At GLA only a 449-MHz profiler was operated, and this radar also collected RASS data. The 449-MHz wind profiler data collected at BBY is referred to as BBY-449 and the 915-MHz wind profiler as BBY-915. For the Goleta site the 449-MHz wind profiler is referenced to simply as GLA. The analysis was performed for the time period from May 1st to August 14th (Julian days 121 to 226), 2006, for both sites.

For wind profiler estimations of the BLD using the fuzzy logic algorithm of Bianco and Wilczak (2002) and Bianceo et al. (2007), we relied on the information obtained by the behavior of signal-to-noise ratio (SNR), variance of vertical velocity, and Doppler spectral width. This automated algorithm was run through the period of interest, and a visual inspection of the algorithm output was performed to remove outliers. The visual inspection was performed using three-panel display plots that illustrate the behaviour of range-corrected SNR, vertical velocity, and Doppler spectral width. About 30% of the algorithm-estimated BLDs were adjusted by visual inspection. For non-coastal sites the automated algorithm has been shown to provide more robust estimates of the depth of the turbulent, convective planetary boundary layer.

For RASS estimations of the BLD, we considered the virtual temperature, T_v, profile taken during the first five minutes of each hour to provide an hourly estimate of the BLD. We converted T_v to virtual potential temperature, θ_v, and found the first point in the θ_v profile at which the value of the gradient of θ_v as a function of height is less than 0.3 ^{o}C km^{-1}. The altitude of the lower bound used in the gradient calculation was estimated to be the BLD. This θ_v gradient threshold was chosen because it best matched the BLD estimates produced when a clearly defined BLD was detected by the automated algorithm. However, often the lapse rate was stably stratified below our RASS estimate of the BLD. This stable layer may have been intermittently turbulent, or it may have exhibited primarily laminar flow.

Figure 4.3-1 shows an example of BLD estimations calculated on Julian day 136 (May 16) by the two wind profilers at BBY. Because the marine boundary layer is often only a few hundred meters deep, the finest vertical resolution data collected by each wind profiler were used. For the BBY-915, this corresponds to 63-m vertical resolution, while for the BBY-449 this corresponds to 106-m vertical resolution.

Figure 4.3-2 is a scatterplot comparison of the BLD estimations for the entire analysis period when both profilers detected a BLD. Statistical results are shown in the upper right hand corner of the figure. The number of BLD estimations provided by the BBY-449 (1307) is greater than the number of BLD estimations provided by the BBY-915 (969). The first reason for this disparity is the BBY-449's greater sensitivity to atmospheric turbulence, as demonstrated in the previous Section by Fig. 4-2.2. The second reason is the greater altitude coverage provided by the BBY-449, which gives the automated algorithm more data with which to determine the BLD. The air above the marine boundary layer along the West Coast of the U.S. is particularly difficult for the BBY-915 to observe because it is very dry and the

wavelength is comparatively smaller (versus the BBY-449) to the inner scale of turbulence. The scatterplot also shows that there were a number of occasions when the BLDs measured by the BBY-915 were below the BLDs measured by the BBY-449. This behavior occurred when the boundary layers were shallow, which gave the BBY-915 two advantages because of its increased vertical resolution and lower minimum detectable range as compared to the BBY-449 (see Table 2.2-1). This occurred approximately 15% of the time during the analysis period.

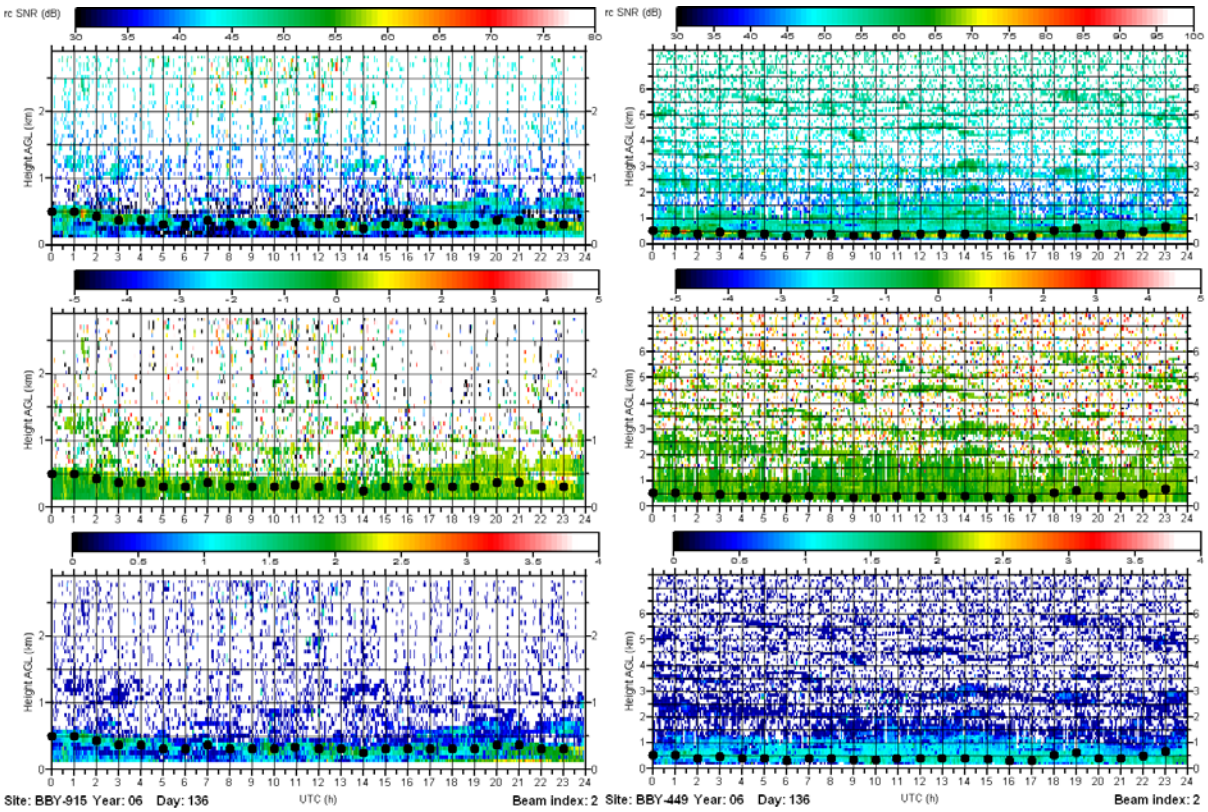

Figure 4.3-1 BBY-915 (left) and BBY-449 (right) time-height cross sections of vertical beam Doppler spectral moments for Julian day 136. Top panel: range-corrected SNR; middle panel: vertical velocity; lower panel: Doppler spectral width. The black dots denote BLD estimations produced by the automated algorithm.

For the 449-MHz wind profiler and RASS at GLA, we performed the same analysis with the Doppler spectral moments using the automated algorithm and compared the results with BLD estimations derived from profiles of the virtual potential temperature, θ_v, measured by the RASS. This latter method worked well except for cases where the inversion extended down to the surface. For these very stable conditions, a clearly defined BLD is often difficult to determine (Vickers and Mahrt, 2004). Figure 4.3-3 shows the BLD estimations for two days derived using the RASS θ_v profiles. When a well-defined inversion is present, the BLD is readily apparent in the RASS profiles. Figure 4.3-4 compares the BLD estimations based on the two methods used for the same two days. The two methods agree when a local peak in

the turbulence profile coincides with the top of the boundary layer. This is the case, for example, with the classic stratocumulus-topped marine boundary layer (e.g., White et al., 1991). However, when clouds that are likely the result of continental processes exist above the marine inversion, the automated algorithm deviates from the RASS method because of the enhanced turbulence in the clouds, e.g. after 16:00 UTC on Julian day 129 (Fig. 4.3-4).

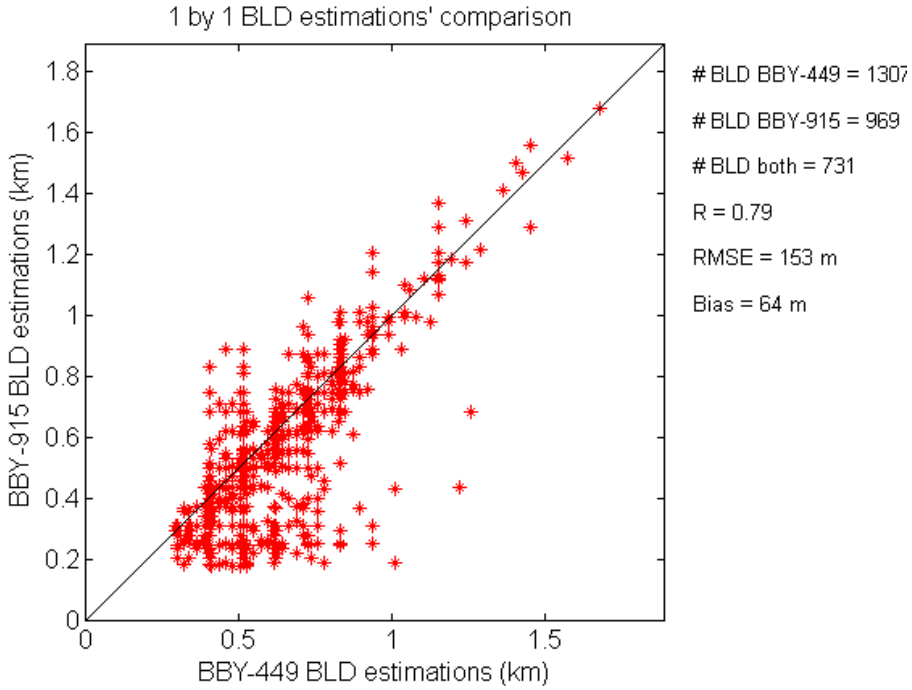

Figure 4.3-2 A scatterplot of boundary-layer depth (BLD) estimations by the BBY-449 and BBY-915 wind profilers.

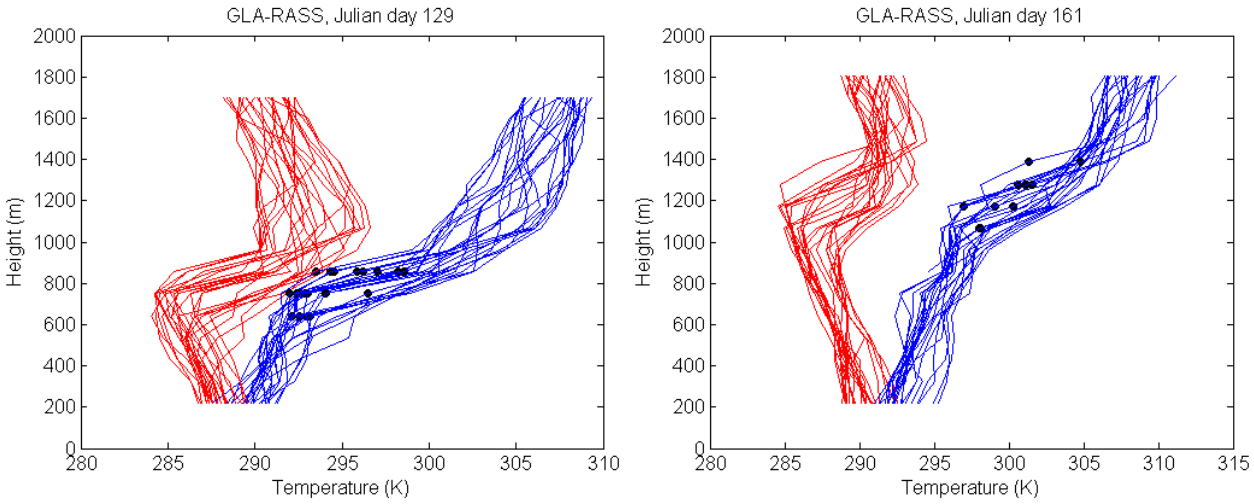

Figure 4.3-3 Hourly vertical profiles of virtual temperature (T_v; red) and virtual potential temperature (θ_v; blue) derived from RASS measurements at GLA on Julian day 129 (left) and Julian day 161 (right). The black dots denote the BLD estimations based on the gradient threshold described in the text.

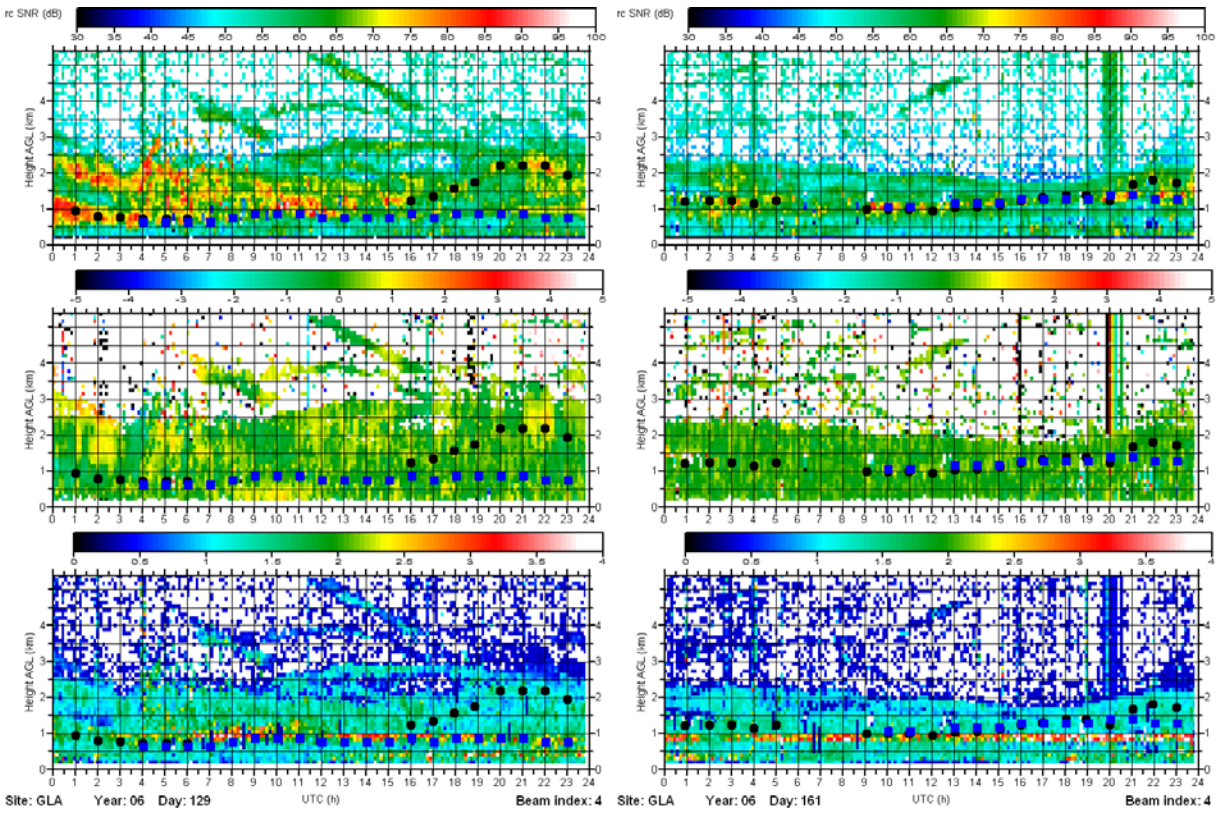

Figure 4.3-4 Time-height cross sections of vertical beam Doppler spectral moments measured by the GLA wind profiler for Julian days 129 (left) and 161 (right). Top panel: range-corrected SNR; middle panel: vertical velocity; lower panel: Doppler spectral width. The black dots denote BLD estimations produced by the automated algorithm and the blue dots denote BLD estimations from the virtual potential temperature profiles measured by the RASS.

Figure 4.3-5 compares the BLD estimates produced by the two methods for the entire evaluation. In many cases, the BLD estimates obtained by the automated algorithm are above the inversion detected by the RASS. As demonstrated by Fig. 4.3-4, we believe this is due to clouds existing above the marine inversion.

By examining the entire evaluation dataset we determined that the 449-MHz RASS data provides a superior method for determining the depth of the marine inversion, except for very stable marine boundary layers, where the inversion extends below the minimum detectable range of the wind profiler. Unfortunately, this occurred 40-50% of the time during the evaluation, indicating that wind profilers are not the optimum technology to use for shallow marine boundary-layer depth detection. The overall data quality of the 449-MHz RASS profiles is much better than the 915-MHz RASS profiles and because of its physical setup, including antenna separation and lower acoustic wavelength, the 449-MHz RASS provides much deeper height coverage than the 915-MHz RASS (see Section 3).

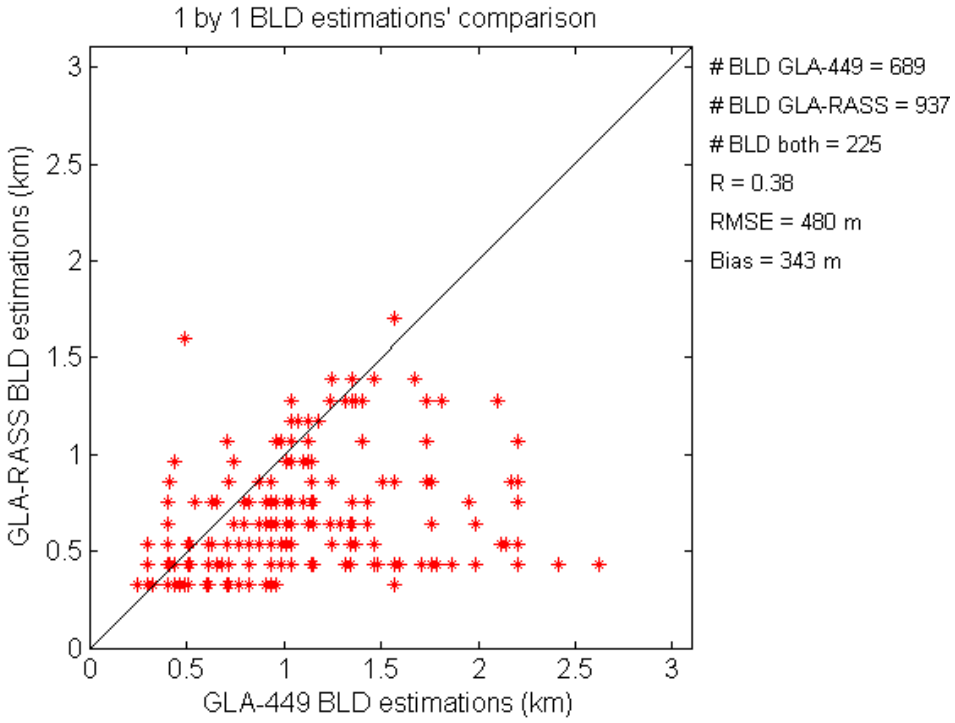

Figure 4.3-5 Scatterplot comparing the BLD estimates provided by GLA-449 using the automated algorithm (horizontal axis) and using the RASS θ_v gradients (vertical axis).

4.4 End-user Feedback

Based on prior experience gained in field research programs that utilized wind profilers, we anticipated that the primary end user of the wind profiler data collected during the IOOS wind profiler technology evaluation would be the NWS Weather Forecast and River Forecast Offices in the local areas where the instruments were deployed. Therefore at the start of the evaluation, we contacted and/or visited the Los Angles/Oxnard Weather Forecast Office, the San Francisco/Monterey Weather Forecast Office, and the California/Nevada River Forecast Center in Sacramento to provide training on the forecast applications of wind profiler data products and to solicit feedback on forecaster's usage of the products in their daily forecast operations. Because the latter two offices had already received training during previous research field campaigns (CALJET, PACJET, HMT), only the LA/Oxnard Forecast Office was visited in person. Realizing that providing feedback could impose an undue burden on forecasters, we attempted to make the process as easy as possible by using web-based feedback forms that appeared side-by-side with the data products. An example of the form that appeared when a forecaster accessed one of the wind profiler data products through ESRL's data web page is shown in Fig. 4.4-1.

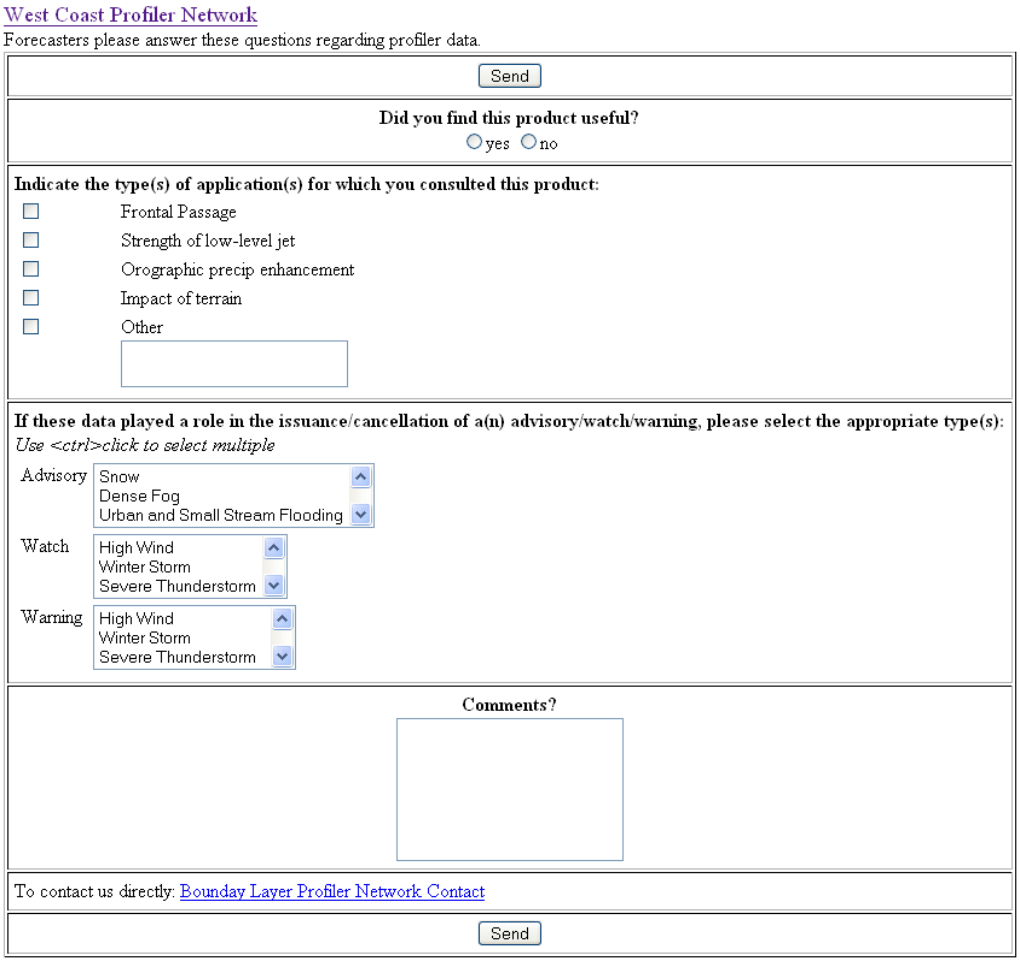

Figure 4.4-1 Example of the web-based form used to collect feedback from NWS forecasters on the use of wind profiler data products during daily forecast operations.

After a forecaster filled out the form and pushed "send," the data from the form were automatically sent and stored on a computer at ESRL. An example that illustrates the type of feedback that was logged during the evaluation is shown in Fig. 4.4-2.

Feedback responses such as the one shown in Fig. 4.4-2 were compiled for the entire evaluation. A total of 31 individual responses were received in reference to the two evaluation sites (BBY and GLA). Of these, three responses did not specify an application for how the data were used. The forecast applications for the remaining 28 responses are shown in Fig. 4.4-3 along with the number of responses for each specific application. Three of the responses indicated that the data were used to issue or cancel a wind advisory and three other responses were used to issue or cancel a snow advisory. In two of the responses, including the one shown in Fig. 4.4-2, the comments indicated that the wind profiler data helped inform forecasters of the depth and severity of low-level wind shear for terminal aviation forecasts (TAFs).

May 25, 2006								
Office	Time (UTC)	Product	Site	Useful?	Applications	Other Applications	Advisories, Watches, Warnings	Comments
204.228.180.83 204.228.180.83	00:58	Signal to Noise Ratio	Goleta	yes	Frontal Passage Strength of low-level jet Orographic precip enhancement Other x terrain_impact	Looking for low level wind shear due to strengthening northerly winds aloft. Data confirmed that the wind shear was developing...but not severe enough to be concerned about at this time.	**Advisory** **Watch** **Warning**	Observation played a role in determining if LLWS was needed in the VNY and BUR TAFs.

Figure 4.4-2 Example of wind-profiler evaluation feedback received from the LA/Oxnard Weather Forecast Office (identifiable by the IP address shown under the "Office" heading) on May 25, 2006. In this case, the forecaster accessed a display of the wind-profiler data that showed the observed wind profiles overlaid on a color background indicating the signal-to-noise ratio of the radar's received signals.

Quite surprisingly, there were also 22 responses from the general public, who like NWS forecasters, were given the opportunity to provide feedback when they accessed the profiler data products on the ESRL web pages. Of these responses, two did not specify an application for how the data were used. The remaining 20 responses indicated that the data were used for air quality applications, current weather, fire weather, marine navigation, public safety, recreation, and research. In particular, we received feedback from an end user who wrote that profiler data were used for "illustrating marine layer and winds aloft for wildfire behavior training materials on relevant fire weather processes. In addition, firefighters are urged in the training to routinely consult the profiler information to help portray the fire weather situation."

One of our goals in soliciting feedback was to obtain quantitative information on the impact of profiler data on the watch/warning program in the form of one or more of the following performance measures: probability of detection, false alarm rate, and lead time. We failed to collect enough of this type of information to be statistically meaningful for two primary reasons. First, during the period surrounding the time when a warning gets issued, forecasters are quite busy gathering information, notifying emergency managers, updating NWS web pages, etc., so it is less likely that they would take the time to fill out the wind profiler evaluation form. Secondly, wind profiler data products may play a role in making a watch/warning decision, but it is just one of the many tools that forecasters rely on in addition to their own judgment. Therefore, much of the feedback we received was more anecdotal in nature.

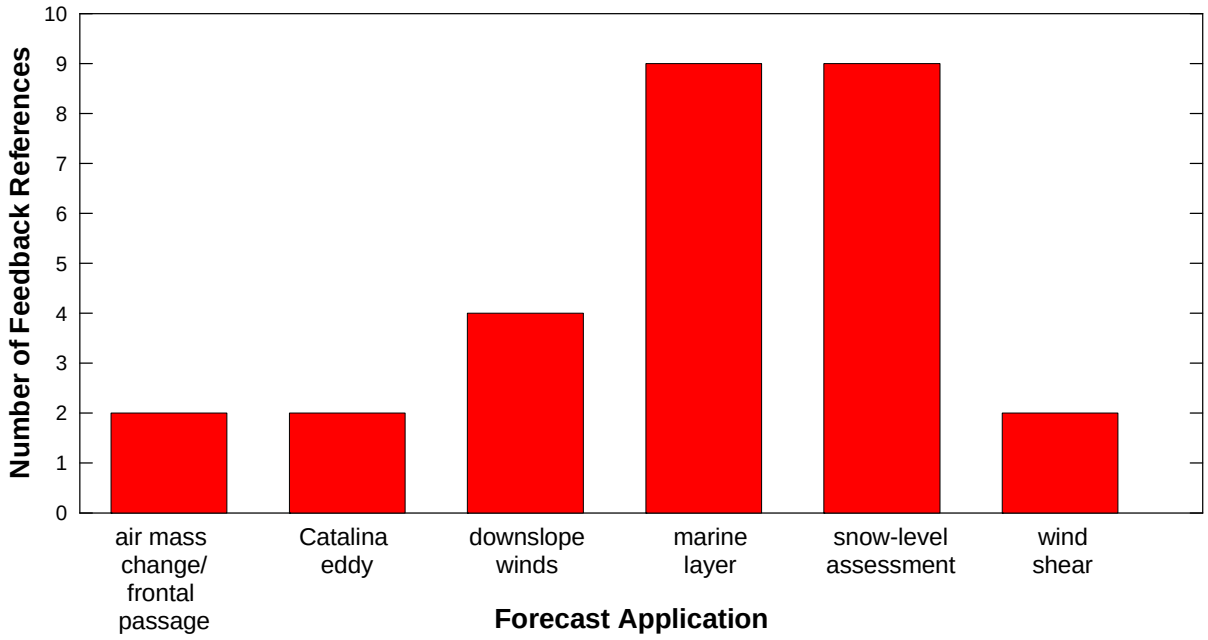

Figure 4.4-3 Forecast applications for wind profiler data identified by NWS forecasters in the LA/Oxnard and San Francisco/Monterey Weather Forecast Offices who accessed profiler data in real time from ESRL's profiler data web pages.

We also personally contacted Dave Reynolds, Meteorologist-In-Charge (MIC) at the San Francisco/Monterey Weather Forecast Office and Dave Danielson, Science and Operations Officer (SOO) at the LA/Oxnard Weather Forecast Office to get their final impressions on how the IOOS-sponsored wind profiler data were used in forecast operations and in the case of BBY, which profiler technology was most useful for marine and coastal weather applications. The impressions of Mr. Reynolds are shown below, followed by the impressions of Mr. Danielson.

****

Mr. Reynolds, which profiler technology at BBY is better suited to coastal weather forecasting?

"There are two key phenomena that we use BL Wind Profiler data for -

Land Falling jets - It would appear that for this phenomena that the 449-MHz profiler provides the best data. It can observe the upper level jet that is coupled with the onset of the highest low level winds associated with the LLJ ahead of surface fronts. Since the LLJ is about 1 km AGL the 449-MHZ profiler can detect the LLJ adequately. Also there is sufficient vertical resolution to identify it as a LLJ based on the definition given by Marty Ralph in the 2005 paper. Because these are larger scale systems the 449-MHz is sufficient. The magnitude of the LLJ is important in estimating the condensate supply rate and thus an estimate of precipitation rate to be expected, especially in orographically favored areas. Remember it is rate not volume we are more concerned about.

Marine Inversion and Coastal Jet - The marine inversion is detected in two ways. The S/N ratio can usually detect the base height of the inversion but climatologically in the summer it is located at 1000 to 1500 ft or 300 to 500 m MSL. The 915-MHZ profiler, given it has 60 m resolution and thus can obtain data at lower altitudes to better resolve the inversion, is the best choice for summer applications. Also RASS is of great benefit for resolving the marine depth. It is superior to the S/N ratio as it is a direct measure of the Tv which is perfect for resolving marine inversions."

Mr. Reynolds, how important are upper air winds compared to surface winds for coastal weather forecasting?

"As mentioned, the upper winds are important during landfalling winter systems, mainly to locate the upper jet core and its passage. We do use the winds at 2 to 5 kft during fire weather season to identify the depth and extent of offshore flow. The RASS data is also very useful combined with the winds to show the warming taking place due to subsidence."

Mr. Reynolds, about how often do forecasters in your office use profiler data to help make decisions about coastal weather forecasts?

"Profiler data is looked at daily in the summer season to track the marine layer...both using S/N and RASS Tv. We also look at the strength of the coastal jet as it can be useful for small craft advisories. But generally we are tracking the depth of the marine layer. This is critical to aviation and temperature/RH forecasts. In winter we monitor the profiler data as storms approach. We look for the depth of the blocking flow to determine where the most concentrated precipitation might be as it can sometimes be near shore or offshore due to convergence. We can monitor warm frontal passage and note that the precipitation max moves onshore and usually into the favored orographic areas once this occurs. It is important that a surface station be collocated with the profiler so the forecaster can see how this is manifested in the surface state parameters."

Mr. Reynolds, would offshore lower tropospheric wind profile observations be more useful than surface observations for coastal weather forecast applications?

"We know that the current NCEP data assimilation system is much more impacted by lower tropospheric soundings than by surface observations. I believe these offshore profiles would need to be several hundred miles offshore to provide both a predictive capability (lead time) and to help initialize the models where data is lacking."

****

Mr. Danielson, why is the wind profiler at Goleta important, and how are the data used in daily forecast operations?

"1. It is a key site for detecting strong **Sundowner wind events** which frequent the south coast of Santa Barbara. Knowing the strength of the winds in this region not only facilitates the issuance of **wind advisories and warnings** for the south coast, but also provides an important site for critical decisions regarding **red flag fire weather conditions** in the mountains of Santa Barbara--one of the driest areas of Southern California during fire season.

2. The Goleta site was also used for forecasting the **depth and likely persistence of the marine layer** which influences the region for about 8 months of the year. Again, knowing the marine layer depth and how it varies on a 24 hour basis is **critical to fire fighting operations** and is a key part of each fire weather and spot forecast we issue. In addition, an accurate marine layer depth forecast is also very important for aviation safety. The low clouds and fog associated with the marine layer produce **LIFR, IFR and MVFR conditions** at Santa Barbara Airport--directly impacting the **safety of air operations**. In addition, profiler winds can be used to more accurately **predict the onset, duration, and height of low level wind shear** at Santa Barbara Airport--which accompanies virtually all Sundowner wind events and many weaker wind events, as well.

3. During winter storms, the Goleta site **fills a critical gap in wind coverage** south of the Santa Ynez Range. Specifically, this is one of the few sites that can tell us whether or not a **barrier jet** has formed and what strength it carries--key information for **QPF forecasting** since the barrier jet can significantly reduce the rainfall rates that we see over water on radar before storms come ashore. In addition, the Goleta site would provide **improved wind coverage** in a region that cannot be effectively monitored by either the Vandenberg or the Sulphur Mountain radars due to the intervening Santa Ynez Mountains."

Finally, the following comments were submitted by Mr. Danielson in response to the Zaca wildfire which burned in Santa Barbara County for much of the summer of 2007.

"1. The statement that the mountains of SBA County were some of the driest areas in Southern California certainly turned out to be prophetic with the recent ZACA fire. That fire started on the 4th of July and wasn't contained until September 2nd. It burned just under a quarter million acres and, so far, has cost about $120M. At times, firefighters estimated flame lengths of 400-500 feet in length. On several days, the fire produced large pyro-cumulus clouds that could be seen from over a hundred miles away. Right in the middle of the fire, Vandenberg AFB cut back from two to one radiosonde a day to save money. So, the Goleta profiler became an even more important source of data. As you can imagine, marine layer depth information was critical since humidities above the marine layer were falling to the low single digits.

2. Fire Departments along the south slopes of the Santa Ynez Range were especially concerned that ZACA might take aim at the Cities of Santa Barbara, Montecito and Carpenteria. All the fire had to do was turn south for a couple hours to cross the Santa Ynez River. If this had happened, the fire would have swiftly spread up the north slopes of the Santa Ynez Range in probably a matter of minutes. These flames would have been capable of putting enough flaming debris into the air to spawn numerous spot fires on the south facing slopes of the Santa Ynez Range which would be hugely problematic for the fire

fighters. Due to the concern for Sundowner Winds, fire officials of the communities on the south slopes requested several "spot" forecasts dealing specifically with the details of the expected Sundowner Winds. The Goleta profiler is pretty well perfectly sited for monitoring these winds. In fact, if you look at last nights data, you can see a pretty good example of a Sundowner wind event in the profiler data.

3. When the rains return this winter [perhaps I should be saying "If" the rains return this winter], we will be looking to the Goleta profiler to help us out with QPF and snow level forecasts. Considering the size of the fire, we could be in for a real mess with mud and debris flows--especially considering that the area that burned is also one that gets hammered by heavy rains from Pacific storms."

****

We are extremely grateful for the feedback we received from NWS staff and for their willingness to participate in this project.

5.0 Acquisition, Operation, and Maintenance Issues

For the IOOS wind profiler technology evaluation, ESRL provided its own 915-MHz wind profiler with RASS for the Bodega Bay site and its own 449-MHz wind profiler with RASS for the Goleta site. Part of the IOOS funding received was used to refurbish the 449-MHz profiler for the evaluation project. In addition, a combination of equipment provided by ESRL and Vaisala, Inc., was used to field the 449-MHz wind profiler for the Bodega Bay site. Without the participation and cooperation of Vaisala, Inc., the project would have been delayed by many months. NOAA used its own profiler at Goleta knowing that the equipment would remain there after the technology evaluation project in support of the NOAA Coastal Storms Program's Southern California Pilot Study, which helped fund the installation of the Goleta profiler in 2005.

5.1 Acquisition Cost

The following table lists the costs that would be required to acquire, operate, and maintain the wind profilers used in the technology evaluation. These costs were provided by Vaisala, Inc., the commercial manufacturer of the wind profiler technologies used in the evaluation, and are based on the General Services Administration (GSA) price schedule. These prices do not include the cost of installation, which varies depending on location. Operation and maintenance are based annually.

Table 5.1-1 Costs ($k) required to acquire, operate, and maintain the commercial versions of the wind profilers used in the IOOS wind profiler technology evaluation

IOOS profiler name: **Commercial version:**	**915-MHz wind profiler** **(LAP®-3000)***	**915-MHz wind profiler with RASS** **(LAP®-3000)***	**¼-scale 449-MHz wind profiler** **(LAP®-8000)**	**¼-scale 449-MHz wind profiler with RASS** **(LAP®-8000)**
Acquire (hardware)	240	280	535	600
Acquire (software)**	20	20	20	20
Operate and maintain	24	24	53	53

* The Vaisala, Inc. LAP®-3000 boundary-layer wind profiler typically operates at either 915 or 1290 MHz.

** Both the research and commercial versions of the profilers used in this study use the LAP-XM® radar control and data acquisition software.

5.2 Operation and Maintenance Issues During the IOOS Campaign

Whether it was good fortune, outstanding engineering, or a combination thereof, the wind profilers used in the IOOS technology evaluation operated continuously without a single failure during the entire 11-month evaluation. This is remarkable given that some of the radar equipment deployed at Bodega Bay had been in use since the early 1990's. Aside from regular on-site maintenance trips performed to ensure that all systems were operating properly, one engineering trip was required in October 2005 to replace an amplifier on the 449-MHz radar receiver in order to reduce recovery spurs (receiver artifacts in the Doppler velocity spectra from which the winds are estimated) that sporadically prevented the wind profiler from producing reliable wind data in its lowest range gates. It is likely for this reason that the lowest range gate of the 449-MHz wind profiler did not report reliable wind data as often as the 915-MHz wind profiler (see Figs. 3.1-1 and 3.1-3).

5.3 Long-term Operation and Maintenance Issues

Wind profilers are all-weather instruments that have a proven track record of performance in a variety of climatic conditions ranging from the poles to the tropics. Based on the experience of ESRL engineering staff, more severe climates – especially wetter climates – can negatively impact the lifespan of the some the wind profiler's major components. For example, leakage of rainwater into the antenna can cause serious damage and ruin instrument performance. The radar antennas used in the wind profiler technologies evaluated in this project are very different. The 915-MHz wind profiler uses a microstrip-patch phased-array antenna that can crack and allow water to penetrate and ruin the integrated circuitry. The 449-MHz wind profiler uses collinear-coaxial antenna elements that also can be subject to leakage. These antenna elements also require a dry-air system in order to maintain steady performance of the antenna under changing environmental conditions. ESRL engineers have estimated the lifetime of the dry air system to be 3-5 years. Otherwise, the lifetime of either type of antennas is on the order of 15 years. In addition, both types of profilers used in the technology evaluation require switches in order to change the beam orientations for wind profiling. These switches have a lifetime of about 2-5 years.

6.0 Frequency Security

6.1 Licensing Requirements for Wind Profilers

All U.S. government frequency allocations are assigned by the National Telecommunications and Information Administration (NTIA), while civilian frequency allocations are assigned by the Federal Communications Commission (FCC). NTIA issues licenses for the operation of any federal transmitting device. The allocations and rules are contained in the Manual of Regulations and Procedures for Federal Radio Frequency Management available on the Internet at http://www.ntia.doc.gov/osmhome/redbook/redbook.html. There are three types of licenses that govern wind profiler operations: experimental, stage three, and operational. In addition, the FCC allows small power (up to 1 Watt) transmitters to operate as Part 15 devices. A large number of devices operate under these rules (e.g., wireless phones and radio modems). Part 15 devices operate without any legal protection; they cannot interfere with any other device and must accept any interference.

An experimental license allows a wind profiler to be operated on a non-interfering basis. If the profiler interferes with a stage three or operational system, it must be shut down. Also, the profiler operator must accept any interference from stage three or operational systems in use near the wind profiler. During the IOOS wind profiler technology evaluation, NOAA operated the 449-MHz wind profiler at Bodega Bay on an experimental license. This license allows NOAA to operate any number of profilers in the U.S. and its possessions with the requirement that NOAA coordinate with the Military for locations near certain bases. Since the 449-MHz profiler at Bodega Bay was licensed as an experimental system, it did not have to meet the otherwise more stringent frequency specifications required for an operational system.

A stage-three license is granted to systems that are beyond experimental and are working toward operational use. Stage-three system operators can force experimental operators to shut down in order to eliminate interference problems. NOAA has a stage-three license for 915-MHz wind profilers that is good throughout the U.S. and its possessions. The 902-928 MHz band is allocated to Instrumentation, Science, and Medicine (ISM) and is often called the “garbage band.” The ISM band contains a large number of users that cause Radio Frequency Interference (RFI) for wind profilers. Theoretically, these devices, which operate under Part 15 of the FCC code, can be forced to shut down if they interfere with 915-MHz profiler operations. However, there are so many users in this band that removing all illegal, interfering, transmitting devices would not be possible realistically. This is the reason NOAA has never pursued acquiring an operational license for their 915-MHz profilers. Currently, RFI in the 902-928 MHz ISM band practically limits the locations where 915-MHz profilers can operate, and the problem will get even worse in the future.

An operational license is typically issued with limitations on the systems specifications. The owner of an operational license legally can shut down any system that interferes with it, and the operators of other systems in the area must accept any interference that the operational system produces. Currently, there are only five operational 449-MHz wind profilers in the U.S.: three in Alaska, one in Colorado, and one in New York. These wind profilers are part

of the NOAA Profiler Network (NPN). An operational license is issued for only one location so each of these profilers has a separate license to permit its operation. In addition, a profiler with an operational license must meet the requirements specified by NTIA Radar Spectrum Engineering Criteria (RSEC) E. This criterion explicitly describes the allowable radiation spectrum. The ¼-scale 449-MHz wind profiler operating modes used at Bodega Bay during the technology evaluation did not meet RSEC E. This issue needs to be resolved in order for this profiler technology to be able to provide 106-m vertical resolution legally on an operational basis.

The frequency band 420-450 MHz is a Military band that is shared with amateur radio. However, the Military has priority in the band. Wind profilers have been given a shared allocation with amateur radio in the 448-450 MHz band. Both amateur radio operators and wind profiler operators must accept interference from each other. If the Military ever required use of the band, both wind profiler operators and amateur radio operators would be required to shut down their equipment.

7.0 Summary and Discussion

7.1 Summary

This report evaluated two current state-of-the-art wind profiler technologies as potential candidates to fill an important gap in NOAA's Integrated Coastal Ocean Observing System (ICOOS). Coastal and marine weather monitoring and prediction suffer from a lack of in situ upper-air wind and temperature observations, and wind profilers have been identified as a cost-effective technology to provide this critical information to the National Weather Service and other end users.

The technology evaluation took place at the University of California's Bodega Bay Marine Laboratory in Sonoma County and at the Santa Barbara Airport in Goleta, Santa Barbara County. Side-by-side operation of a ¼-scale 449-MHz wind profiler and a 915-MHz boundary-layer wind profiler with a radio acoustic sounding system (RASS) occurred at Bodega Bay from mid-September 2005 to mid-August 2006. Operation of a ¼-scale 449-MHz wind profiler with RASS occurred at Goleta during the same time period. The Goleta wind profiler and RASS were also supported by NOAA's Coastal Storms Program. Because RASS systems operating at the different profiler frequencies could not be run simultaneously at either evaluation site, a 915-MHz RASS dataset collected at Goleta during the same time period in 2001-2002 was used in the evaluation of Goleta RASS performance.

Each wind profiler technology was evaluated based on its operating performance (e.g., minimum and maximum altitude coverage) and its ability to detect and monitor key coastal weather phenomena. Other topics that were addressed in this report were acquisition cost, operation and maintenance issues, and frequency security. The primary findings of these analyses were reported in the Executive Summary Section. Details pertaining to operating performance, cost, and operation and maintenance issues were described in Sections 3 and 5. Objective analyses of how well each wind profiler was able to detect and monitor important coastal weather phenomena in addition to feedback received from National Weather Service staff were described in Section 4. Issues related to frequency security were identified in Section 6.

7.2 Discussion

Both wind profilers performed admirably during the technology evaluation, so with respect to their ability to provide continuous data throughout all seasons, there was not an advantage to using either technology. In addition, the evaluation was not long enough (11 months) to determine the long-term operating sustainability of either technology.

For wind profiling, the primary advantage of the ¼-scale 449-MHz wind profiler was extended altitude coverage (more than three times that of the 915-MHz wind profiler). This coverage is important for providing wind data for assimilation into numerical models and because it fills the gap between the surface, where relatively dense observing networks exist, and roughly 500 mb, where there is an increasing number of automated aircraft

measurements available. The analyses showed that the 449-MHz profiler's minimum detectable altitude was adequate to capture important, shallow coastal weather phenomena such as gap flow. The increased sensitivity of the 449-MHz frequency to scattering from atmospheric turbulence relative to its sensitivity to scattering from hydrometeors meant that the 449-MHz wind profiler did not perform as well as the 915-MHz wind profiler for snow-level detection. However, the small number of cases for which this was true, combined with the light rainfall that accompanied these events, indicated that for hydrometeorologically significant rainfall events, the 449-MHz wind profiler's performance in detecting the snow level was sufficient.

Again, for wind profiling, the primary advantage of the 915-MHz wind profiler was minimum altitude coverage and vertical resolution. The 915-MHz profiler detects winds at a lower minimum altitude (110 m vs. 185 m above ground level). This increased low altitude coverage and enhanced vertical resolution (63 m vs. 106 m) allowed the 915-MHz profiler to better resolve the wind jet associated with gap flow. In addition, the enhanced vertical resolution combined with the absence of clear-air turbulence signals during precipitation meant that the 915-MHz wind profiler did a better job detecting the snow level, especially for lower-altitude snow levels and in light precipitation events. Because of its limited coverage above the boundary layer, the 915-MHz wind profiler leaves a significant gap in altitude coverage between the boundary layer and the middle troposphere, where flight-level automated aircraft observations exist.

For temperature profiling via the RASS technique, it was clear that the 449-MHz RASS outperformed the 915-MHz RASS both in terms of maximum altitude coverage and data quality. The RASS profiles provide a superior method for detecting the inversion capping the turbulent coastal marine boundary layer as compared to the automated algorithm that was developed for detecting the depth of the convective planetary boundary layer (Bianco and Wilczak, 2002; Bianco et al., 2007). For more stable boundary layers that are shallower than the minimum detectable range of the RASS or where the inversion extends to the surface, there does not appear to be an optimal way to measure the depth of the coastal marine boundary layer using either wind-profiler technology. In fact, for the latter case, research has shown that there often is not a robust definition of boundary-layer depth. For the very shallow coastal marine boundary layers that can exist along the entire West Coast, or in the Gulf of Maine for example, sodar is perhaps the best possible technology to use (e.g., White et al., 1991). For locations where the depth and strength of the boundary layer are of primary importance, a sodar operating in conjunction with a wind profiling radar would create a powerful integrated observing tool. At the time of this report, two sodars were a critical component of the San Francisco Airport Marine Stratus Forecast System (Ivaldi et al., 2006).

The 449-MHz and 915-MHz wind profiler technologies are both commercially available. The 449-MHz wind profiler with RASS is approximately twice as expensive as the 915-MHz wind profiler with RASS (see Section 5.1 for details). In addition the estimated annual expense of operating and maintaining a 449 MHz wind profiler is about twice the amount of operating and maintaining a 915-MHz wind profiler.

Perhaps the most serious challenge with respect to making either technology operationally viable is frequency security. Here the 449-MHz wind profiler has a clear advantage because the National Telecommunications and Information Administration has allocated the 448-450 MHz frequency band to wind profilers and amateur radio operators, although the Military is considered the primary operator in this frequency band. The 915-MHz profiler operates in the crowded band from 902-928 MHz that has been allocated to Instrumentation, Science, and Medicine. Even though NOAA has a stage-three license to operate wind profilers in this band, the radio frequency interference (RFI) that exists today already is limiting the locations where 915-MHz wind profilers can be deployed practically, and the problem is forecast to get even worse in the future.

Finally, it makes logistical sense for all of NOAA's operational wind profilers to operate at the same frequency. In this case the 449-MHz wind profiler technology would be preferred for coastal applications because 449 MHz will be the new operating frequency of the NOAA Profiler Network (NPN) wind profilers located primarily in the central part of the U.S. However, unless the new NPN technology is able to provide higher resolution profile data and improved minimum detectable range than its predecessor, then this technology will not be suitable for coastal weather applications. Ultimately, what may be required is a scalable wind-profiler technology, one that will allow the meteorological forecast problems for which the observed data are intended to dictate how the technology is optimized for a particular region. Clearly, technology assessments such as this one funded by the Integrated Ocean Observing System are necessary before adopting a "one-size-fits all" strategy for future enhancements to the Nation's coastal observing system.

8.0 Bibliography

Batton, L.J., 1973: *Radar Observations of the Atmosphere*. University of Chicago Press, Chicago, Illinois, 323 pp.

Bell, G.D., and L.F. Bosart, 1988: Appalachian cold-air damming. *Mon. Wea. Rev.*, **116**, 137-161.

Bianco, L., and J. M. Wilczak, 2002: Convective boundary layer mixing depth: Improved measurement by Doppler radar wind profiler using fuzzy logic. *J. Atmos. Oceanic Technol.*, 19, 1745–1758.

Bianco, L., J. M. Wilczak, and A. B. White, 2007: Convective boundary layer depth estimation from wind profilers: statistical comparison between an automated algorithm and expert estimations, *(submitted to J. Atmos. Ocean. Technol)*.

Bjerknes, J., and H. Solberg, 1921: Meteorological conditions for the formation of rain. *Geofys. Publ.*, **2**, 1-60.

Bond, N.A., C.F. Mass, B.F. Smull, R.A. Houze, M.-J. Yang, B.A. Colle, S.A. Braun, M.A. Shapiro, B.R. Colman, P.J. Neiman, J.E. Overland, W.D. Neff, and J.D. Doyle, 1997: The coastal observation and simulation with topography (COAST) experiment. *Bull. Amer. Meteor. Soc.*, **78**, 1941-1955.

Bond, N.A., and P.J. Stabeno, 1998: Analysis of surface winds in Shelikof Strait, Alaska, using moored buoy observations. *Wea. Forecasting*, **13**, 547-559.

Bousquet, O., and B.F. Smull, 2003: Observations and impacts of upstream blocking during a widespread orographic precipitation event. *Quart. J. Roy. Meteor. Soc.*, **129**, 391-409.

Braun, S.A., R. Rotunno, and J.B. Klemp, 1999: Effects of coastal orography on landfalling cold fronts. Part I: Dry, inviscid dynamics. *J. Atmos. Sci.*, **56**, 517-533.

Carbone, R.E., W.A. Cooper, and W.-C. Lee, 1995: Forcing of flow reversal along the windward slopes of Hawaii. *Mon. Wea. Rev.*, **123**, 3466-3480.

Colle, B.A., and C.F. Mass, 1995: The structure and evolution of cold surges east of the Rocky Mountains. *Mon. Wea. Rev.*, **123**, 2577-2610.

Colle B. A., and C. F. Mass, 2000: High-resolution observations and numerical simulations of easterly gap flow through the Strait of Juan de Fuca on 9-10 December 1995. *Mon. Wea. Rev.*, **128**, 2398-2422.

Colle, B.A., K.A. Loescher, G.S. Young, and N.S. Winstead, 2006: Climatology of barrier jets along the Alaskan coast, Part II: Large-scale and sounding composites. *Mon. Wea. Rev.*, **134**, 454-477.

Colman, B.R., and C.F. Dierking, 1992: The Taku wind of southeast Alaska: Its identification and prediction. *Wea. Forecasting*, **7**, 49-64.

Doyle, J.D., 1997: The influence of mesoscale orography on a coastal jet and rainband. *Mon. Wea. Rev.*, **125**, 1465-1488.

Doyle, J.D., and N.A. Bond, 2001: Research aircraft observations and numerical simulations of a warm front approaching Vancouver Island. *Mon. Wea. Rev.*, **129**, 978-998.

Dunn, L. 1987: Cold air damming by the Front Range of the Colorado Rockies and its relationship to locally heavy snows. *Wea. Forecasting*, **2**, 177-189.

Garner, S.T., 1999: Blocking and frontogenesis by two-dimensional terrain in baroclinic flow. Part I: Numerical experiments. *J. Atmos. Sci.*, **56**, 1495-1508.

Ghebrebrhan, O., 1990: Full decoding of truncated ranges for ST/MST radar applications. *IEEE Trans. Geosci. Remote Sens.*, **28**, 14-18.

Gilliam, H., 1970: *Weather of the San Francisco Bay Region*. University of California Press, 72 pp.

Holets, S., and R.N. Swanson, 1981: High-inversion fog episodes in central California. *J. Appl. Meteor.*, **20**, 890-899.

Ivaldi, C., D. Clark, and D. Reynolds, 2006: Upgrade and technology transfer of the San Francisco Marine Stratus Forecast System to the National Weather Service. *Preprint Vol., 12th Conf. on Aviation, Range, and Aerospace Meteorology,* 30 Jan.–2 Feb., 2006, Atlanta, GA, AMS, Boston.

Jackson, P.L., and D.G. Steyn, 1994: Gap winds in a fjord. Part I: Observations and numerical simulation. *Mon. Wea. Rev.*, **122**, 2645-2665.

Loescher, K.A., G.S. Young, B.A. Colle, and N.S. Winstead, 2006: Climatology of barrier jets along the Alaskan coast, Part I: Spatial and temporal distributions. *Mon. Wea. Rev.*, **134**, 437-453.

Marwitz, J., 1983: The kinematics of orographic airflow during Sierra storms. *J. Atmos. Sci.*, **40**, 1218-1227.

Marwitz, J., and J. Toth, 1993: The Front Range Blizzard of 1990. Part I: Synoptic and mesoscale structure. *Mon. Wea. Rev.*, **121**, 402-415.

Mass, C.F., S. Businger, M.D. Albright, and Z.A. Tucker, 1995: A windstorm in the lee of a gap in a coastal mountain barrier. *Mon. Wea. Rev.*, **123**, 315-331.

Medina, S., and R.A. Houze, 2003: Air motions and precipitation growth in Alpine storms. *Quart. J. Roy. Meteor. Soc.*, **129**, 345-371.

Neiman, P.J., F.M. Ralph, A.B. White, D.A. Kingsmill, and P.O.G. Persson, 2002: The statistical relationship between upslope flow and rainfall in California's coastal mountains: Observations during CALJET. *Mon. Wea. Rev.*, **130**, 1468-1492.

Neiman, P.J., P.O.G. Persson, F.M. Ralph, D.P. Jorgensen, A.B. White, and D.E. Kingsmill, 2004: Modification of fronts and precipitation by coastal blocking during an intense landfalling winter storm in Southern California: Observations during CALJET. *Mon. Wea. Rev.*, **132**, 242-273.

Neiman, P.J., F.M. Ralph, A.B. White, D.D. Parrish, J.S. Holloway, and D.L. Bartels, 2006: A Multiwinter analysis of channeled flow through a prominent gap along the northern California Coast during CALJET and PACJET. *Mon. Wea. Rev.*, **134**, 1815-1841.

Overland, J.E., and N.A. Bond, 1995: Observations and scale analysis of coastal wind jets. *Mon. Wea. Rev.*, **123**, 2934-2941.

Overland, J.E., and B.A. Walter, 1981: Gap winds in the Strait of Juan de Fuca. *Mon. Wea. Rev.*, **109**, 2221-2233.

Parish, T.R., 1982: Barrier winds along the Sierra Nevada Mountains. *J. Appl. Meteor.*, **21**, 9215-930.

Peters, G., H. Timmermann, and H. Hinzpeter, 1983: Temperature sounding in the planetary boundary-layer by RASS – System-analysis and results. *Int. J. Remote Sensing*, **4**, 49-63.

Peterson, T.C., L.O. Grant, W.R. Cotton, and D.C. Rogers, 1991: The effect of decoupled low-level flow on winter orographic clouds and precipitation in the Yampa River Valley. *J. Appl. Meteor.*, **30**, 368-386.

Sharp J. M., 2002: Columbia Gorge gap flow. *Bull. Amer. Meteor. Soc.*, **83**, 1757–1762.

Sinclair, M.R., D.S. Wratt, R.D. Henderson, and W.R. Gray, 1997: Factors affecting the distribution and spillover of precipitation in the Southern Alps of New Zealand – A case study. *J. Appl. Meteor.*, **36**, 428-442.

Smith, R.B., 1979: The influence of mountains on the atmosphere. *Advances in Geophysics*, Vol. 21, Academic Press, 87-230.

Steiner, M., O. Bousquet, R.A. Houze, B.F. Smull, and M. Mancini, 2003: Airflow within major Alpine river valleys under heavy rainfall. *Quart. J. Roy. Meteor. Soc.*, **129**, 411-431.

Underwood, S.J., G.P. Ellrod, and A.L. Kuhnert, 2004: A multiple-case analysis of nocturnal radiation-fog development in the Central Valley of California utilizing the GOES nighttime fog product. *J. Appl. Meteor.*, **43**, 297-311.

Wang, J.-J., and Y.-L. Chen, 1998: A case study of tradewind rainbands and their interaction with the island-induced airflow. *Mon. Wea. Rev.*, **126**, 409-423.

White, A.B., C.W. Fairall, and D.W. Thomson, 1991: Radar observations of humidity variability in and above the marine atmospheric boundary layer. *J. Atmos. Oceanic Technol.*, **8**, 639-658.

White, A.B., D.J. Gottas, E. Strem, F.M. Ralph, and P.J.Neiman, 2002: An automated bright-band height detection algorithm for use with Doppler radar vertical spectral moments. *J. Atmos. Oceanic Technol.*, **19**, 687-697.

Wilczak, J.M., R.G. Strauch, F.M. Ralph, B.L. Weber, D.A. Merritt, J.R. Jordan, D.E. Wolfe, L.K. Lewis, D.B. Wuertz, and J.E. Gaynor, 1995: Contamination of wind profiler data by migrating birds: Characteristics of corrupted data and potential solutions. *J. Atmos. Oceanic Technol.*, **12**, 449-467.

Weber, B.L., D.B. Wuertz, D.C. Welsh, and R. McPeek, 1993: Quality controls for profiler measurements of winds and RASS temperatures. *J. Atmos. Oceanic Technol.*, **10**, 452-464.

Yu, C.-K., and B.F. Smull, 2000: Airborne Doppler observations of a landfalling cold front upstream of steep coastal orography. *Mon. Wea. Rev.*, **128**, 1577-1603.

Yu, C.-K., and N.A. Bond, 2002: Airborne Doppler observations of a cold front in the vicinity of Vancouver Island. *Mon. Wea. Rev.*, **130**, 2692-2708.